Title: Intermittent fasting promotes ILC3s secreting IL-22 contributing to the beigeing of white adipose tissue.

Running Title: ILC3s and beigeing

Authors: Hong Chen[1,4#], Lijun Sun[1#], Lu Feng[1], Xue Han[1], Yunhua Zhang[1], Wenbo Zhai[1], Zehe Zhang[1], Michael Mulholland[2], Weizhen Zhang[1,2*], Yue Yin[3*]

Affiliations:

1. Department of Physiology and Pathophysiology, School of Basic Medical Sciences, and Key Laboratory of Molecular Cardiovascular Science, Ministry of Education, Peking University, Beijing 100191, China
2. Department of Surgery, University of Michigan Medical Center, Ann Arbor, MI 48109-0346, USA
3. Department of Pharmacology, School of Basic Medical Sciences, and Key Laboratory of Molecular Cardiovascular Science, Ministry of Education, Peking University, Beijing,100191, China.
4. State Key Laboratory of Female Fertility Promote, Center for Reproductive Medicine, Department of Obstetrics and Gynecology, Peking University Third Hospital, Beijing, China.

# These authors contribute equally to the study

***Correspondence:**

Weizhen Zhang

Department of Physiology and Pathophysiology, School of Basic Medical Sciences, Peking University Health Science Center, Beijing 100191, China

E-mail: weizhenzhang@bjmu.edu.cn; Tel: 0086-10-82802183

or

Yue Yin

Department of Pharmacology, School of Basic Medical Sciences, and Key Laboratory of Molecular Cardiovascular Science, Ministry of Education, Peking University, Beijing,100191, China.

E-mail: yueyin@bjmu.edu.cn; Tel: 0086-10-82802514

Author contributions

Weizhen Zhang, Yue Yin and Hong Chen designed the study; Hong Chen and Lijun Sun performed most of the experiments and analyzed the data; Lu Feng, Xue Han, Yunhua Zhang, Wenbo Zhai and Zehe Zhang helped with the experiments; Hong Chen wrote the original draft; Weizhen Zhang reviewed and edited the manuscript; Yue Yin and Weizhen Zhang obtained funding and supervised the study. All authors have read and agreed to the published version of the manuscript.

Competing interests

The authors declare no competing interests.

Acknowledgments

This research was supported by grants from the National Natural Science Foundation of China (81930015, 81730020, 82070592 and 82270610) and National Institutes of Health Grant R01DK112755 and 1R01DK129360.

Data availability

Data that support the findings in this study are available from corresponding authors upon reasonable request.

Abstract

Mechanism underlying the metabolic benefit of intermittent fasting remains largely unknown. Here, we reported that intermittent fasting promoted IL-22 production by ILC3s and subsequent beigeing of subcutaneous white adipose tissue. Adoptive transfer of intestinal ILC3s increased beigeing of white adipose tissue in diet-induced-obese mice. Exogenous IL-22 significantly increased the beigeing of subcutaneous white adipose tissue. Deficiency of IL-22 receptor attenuated the beigeing induced by intermittent fasting. Single-cell sequencing of sorted intestinal immune cells revealed that intermittent fasting increased aryl hydrocarbon receptor signaling in ILC3s. Analysis of cell–cell ligand receptor interactions indicated that intermittent fasting may stimulate the interaction of ILC3s with dendritic cells (DCs) and macrophages. These results establish the role of intestinal ILC3s in beigeing of white adipose tissue, suggesting that ILC3/IL-22/IL-22R axis contributes to the metabolic benefit of intermittent fasting.

Key word:

ILC3s; IL-22; Beigeing of white adipose tissue; Intermittent fasting

Introduction

Obesity is defined as an epidemic metabolic disease characterized by excessive fat accumulation as the consequence of long-term energy surplus. Thus, therapeutic management of obesity has been focused on the restoration of energy balance, either by decreasing energy intake or increasing energy expenditure[1]. Among these strategies, intermittent fasting is becoming a popular dietary approach. All intermittent fasting schemes including alternate day fasting, 5:2 intermittent fasting and daily time-restricted feeding have shown the health benefits such as delaying aging[2-6], improving metabolism[7, 8], and enhancing cognition[9-11]. The mechanism underlying metabolic benefit of intermittent fasting remains largely unknown. Its metabolic benefit was initially attributed to limitation of energy intake. Recent studies have indicated an alternative mechanism involving beigeing of white adipose tissue, which accounts for the major plasticity of energy expenditure. Studies by Kim *et al.* have showed that intermittent fasting induces white adipose beigeing via stimulation of angiogenesis and macrophage M2 polarization[12]. On the other hand, studies by Li *et al.*[13] have indicated that alternate day fasting induces white adipose tissue beigeing by shaping the gut microbiota and elevating the fermentation products acetate and lactate. Although gut microbiota is closely related to immune response, it remains unclear whether intestinal immune cells contribute to the metabolic benefit of intermittent fasting.

Innate lymphoid cells (ILCs) are a group of natural immune cells lacking antigen-specific receptors expressed on T cells and B cells[14]. Based on developmental trajectories, ILCs are divided into five groups: natural killer cells, type 1 ILCs, type 2

ILCs, type 3 ILCs (ILC3s) and lymphoid tissue-inducing cells[15]. Adipose-Resident type 1 ILCs can promote adipose tissue fibrosis and obesity-associated insulin resistance[16, 17] while type 2 ILCs promote beiging of white adipose tissue and limit obesity[18-20]. However, the contribution of ILC3s on adipocytes and obesity are less clear. ILC3s can produce interleukin-17 (IL-17) and interleukin-22 (IL-22) in response to extracellular bacteria and fungi[21]. ILC3s derived IL-22 can enhance the intestinal mucosal barrier function, reduce endotoxemia and inflammation, ameliorate insulin sensitivity[22, 23] and improve the metabolic disorder of polycystic ovary syndrome[24]. However, ILC3s are also reported to be involved in the induction of obesity[25], contributing to the metabolic disease [25-28]. Therefore, the role of ILC3s in metabolic disease seems complex and the role of ILC3s in intermittent fasting and beigeing of adipose tissue is not known.

Here, we showed that alternate day fasting promoted the secretion of IL-22 by ILC3s. Further, adoptive transfer of intestinal ILC3s increased thermogenesis in DIO mice. Exogenous IL-22 induced the beigeing of white adipose tissue. Deficiency of IL-22 receptor attenuated the beigeing of white adipose tissue induced by intermittent fasting. Our study demonstrates that intestinal ILC3-IL-22-IL-22R axis is actively involved in the regulation of adipose tissue beigeing. Our findings thus reveal a novel pathway in the dialog between the gut and adipose tissue.

Results

1. Intermittent fasting enhances IL-22 production by intestinal ILC3s

To explore the effect of intermittent fasting on intestinal immune cells, we applied alternate-day fasting to mice fed normal chow diet (NCD-IF group) or high-fat diet (HFD-IF group) (Fig. 1A). Intermittent fasting significantly reduced the body weight of mice fed HFD, while demonstrating no effect on total food intake (Supplementary Fig. 1A-B). Moreover, intermittent fasting decreased the respiratory quotient (RQ) on the fasting day while increased the energy consumption on the feeding day in mice fed HFD (Supplementary Fig. 1C, D), improved glucose and lipid metabolism in mice fed HFD (Supplementary Fig. 1E, 1F), and promoted white adipose tissue beigeing in mice fed NCD or HFD (Supplementary Fig. 2).

To explore whether gut immune system contributes to the effects of intermittent fasting on white adipose tissue beigeing, we examined levels of various cytokines in intestine. Notably, mRNA level of IL-22 in the NCD-IF group was significantly higher relevant to the control group (Fig. 1B). Consistently, plasma concentration of IL-22 detected by ELISA was also increased (Fig. 1C). These results suggest that intermittent fasting increases levels of IL-22 in the intestine and plasma. Since ILC3s are one of the major sources of IL-22 in mice[29, 30], we detected the proportion of ILC3s in the lamina propria of small intestine using flow cytometry. In mice fed NCD, intermittent fasting significantly increased proportion of IL-22 positive ILC3s in the small intestine lamina propria (Fig. 1D), while demonstrating no effect on the percentile of total ILC3s (Fig. 1E). Interestingly, intermittent fasting did not influence the secretion of IL-22 of T cells marked as Lineage^{+} Rorγ^{+} cells (Fig. 1F). Besides, intermittent fasting didn't alter the levels of ILC3s and IL-22 in mouse adipose tissue (Fig. 1G and Supplementary Fig. 3).

133 Similar to NCD mice, intermittent fasting significantly increased mRNA levels of IL-
134 22 in the intestine of HFD mice while didn't influence the secretion of IL-22 by T cells
135 (Figure 1H-I). Furthermore, mice fed high-fat diet showed an obvious reduction in the
136 plasma IL-22 (Fig. 1J)and percentage of total and IL-22 positive ILC3s (Fig. 1K).
137 Further, the decrement of plasma IL-22 (Fig. 1J) as well as IL-22 positive ILCs in
138 intestine (Fig. 1K) was attenuated by 30 days intermittent fasting.

139 In order to explain the chronological relationship between ILC3s secreting IL-22
140 and beigeing of white adipose tissue, the mice were exposed to one cycle of intermittent
141 fasting for 2 days. At this time, the body weight of mice didn't change and beige
142 adipocytes haven't been induced (supplementary Fig 4 A-B). However, significant
143 increase in proportion of IL-22 positive ILC3s was induced by intermittent fasting for
144 two days whereas total percentile of ILC3s remained unalterd (supplementary Fig 4 C).
145 These results indicate that the beiging of white adipose tissue are subsequent to its effect
146 on ILC3s secreting IL-22.

147 2. Intestinal ILC3s promote beigeing of white adipose tissue

148 Next, we examined whether adoptive transfer of intestinal ILC3s can increase
149 beigeing of white adipose tissue in diet-induced obesity (DIO) mice. Intestinal ILC3s
150 were isolated and purified from the small intestinal lamina propria of NCD mice
151 (Supplementary Fig. 5A). These cells were defined as lineage^{-}CD127^{+}KLRG1^{-}c-Kit^{+}
152 cells (Supplementary Fig. 5B). As shown in Fig. 2A, DIO mice transferred with ILC3s
153 demonstrated a significant increment in the proportion of small intestinal ILC3s.
154 Plasma concentration of IL-22 also increased significantly relevant to PBS control (Fig.

155 2B). Relevant to PBS control, adoptive transfer of intestinal ILC3s decreased body
156 weight and weight of sWAT (Subcutaneous adipose tissue) slightly, while had no impact
157 on food intake and the liver weight (Supplementary Fig 5C-E). In addition, ILC3s from
158 CD45.1 mouse intestinal lamina propria lymphocytes were adoptively transferred into
159 recipient mice, and CD45.1 positive immune cells were significantly increased in
160 intestine but not in adipose tissue in mice transferred with ILC3s (Supplementary Fig.
161 5E), indicating the feasibility of ILC3s adoptive transfer. Notably, DIO mice transferred
162 with intestinal ILC3s showed improved glucose tolerance (Fig. 2C) and decreased
163 levels of random blood glucose (Fig. 2D). Cold exposure experiment showed that DIO
164 mice transferred with intestinal ILC3s maintained significantly higher rectal
165 temperatures during a 6-h cold challenge (Fig. 2E). Consistently, key thermogenic
166 genes in sWAT including *Ucp1* and *Cidea* were significantly increased (Fig. 2F). Size
167 of adipocytes in the sWAT and eWAT was markedly reduced (Fig. 2G-H). Furthermore,
168 differentiated SVF cells co-cultured with intestinal ILC3s in vitro (Fig. 2I)
169 demonstrated a significant increment in the expression of *Ucp1* and *Pparg* (Fig. 2J), as
170 well as a concurrent decrement in the size of lipid droplets (Fig. 2K). On the other hand,
171 co-culture with CD127^{-} cells demonstrated no effect (Fig. 2J-K). The in vitro
172 experiment indicates the direct effect of ILC3s on adipocytes.

173 3. Exogenous IL-22 increases beigeing of white adipose tissue

174 The role of type 3 immunity in DIO and metabolic syndrome is complex. ILC3-
175 derived IL-22 are beneficial in metabolic syndrome[22, 31] but can also contribute to
176 metabolic disease[25-27]. In order to examine the role of promoting beigeing of white

177 adipose tissue of IL-22 in the context of NCD and HFD mice, we intraperitoneally
178 administrated IL-22 at the dose of 4 μg/kg body weight/every other day for 6 weeks
179 into mice fed NCD or HFD. Saline was used as control. Administration of IL-22
180 increased its plasma concentration in mice fed either NCD or HFD (Supplementary Fig.
181 6A). Exogenous IL-22 significantly increased oxygen consumption, carbon dioxide
182 production and energy expenditure in mice fed either NCD or HFD (Fig. 3A-F).
183 Respiratory quotient (RQ) was significantly reduced in mice fed NCD at dark and mice
184 fed HFD at light(Fig. 3G-H). No significant difference was observed for animal activity
185 (Supplementary Fig. 6B). In addition, exogenous IL-22 significantly improved glucose
186 tolerance in mice fed HFD (Fig. 4A). Interestingly, body weight and food intake were
187 not altered (Supplementary Fig. 6C-6D), indicating that the metabolic benefit of IL-22
188 is not dependent on food intake.

189 We next explored the effect of exogenous IL-22 on thermogenesis induced by 4°C
190 cold exposure. Exogenous IL-22 rendered mice fed HFD resistant to core temperature
191 drop induced by cold exposure (Fig. 4B). Relevant to the pale yellow color in the
192 control animals, subcutaneous fat of obese mice treated with exogenous IL-22 appeared
193 dark yellowish (Fig. 4C). The mRNA levels of thermogenic genes such as *Ucp1* were
194 significantly increased by IL-22 (Fig. 4D). Adipocyte size of subcutaneous adipose
195 tissue and epididymal adipose tissue was significantly reduced in the animals treated
196 with IL-22 (Fig. 4E-4F). These observations suggest that intraperitoneal injection of
197 IL-22 promotes the beigeing of white adipose tissue in mice.

198 To determine whether IL-22 can directly act on adipocytes to promote their beigeing,

199 adipose tissue SVF was isolated and induced for beige differentiation. IL-22 at the dose
200 of 100 ng/mL was continuously administered during beige differentiation. IL-22
201 significantly increased SVF beige differentiation evidenced by cell morphology and
202 increment in mRNA levels of genes relevant to thermogenesis, including *Ucp1* and
203 *Cidea* (Fig. 4G-H). These results suggest that IL-22 can stimulate beigeing of white
204 adipose tissue via its direct action on adipocytes.

205 4. IL-22R knock-out blocks beigeing induced by intermittent 206 fasting

207 To explore whether IL-22R mediates the effect of intermittent fasting on the beigeing
208 of white adipose tissue, IL-22R knockout (IL-22RKO) mice and wild-type (WT)
209 littermates were subjected to alternate-day fasting diet for 30 days. Rectal temperature
210 of WT-IF and IL-22RKO-IF mice was monitored during two consecutive days of
211 intermittent fasting. On the fasting day, the rectal temperature of IL-22RKO-IF mice
212 was significantly lower than that of WT-IF mice at 16:00 time point (Fig. 5A). On the
213 feeding day, the rectal temperature of IL-22RKO-IF mice was lower at three time points:
214 8:00, 12:00 and 20:00 (Fig. 5B). These results indicate that IL-22RKO attenuates the
215 thermogenesis induced by intermittent fasting. Knock-out of IL-22R demonstrated no
216 effect on the glucose tolerance and insulin sensitivity in mice fed NCD (Fig. 5C-D).
217 However, the weight of subcutaneous adipose tissue in IL-22RKO-IF mice increased
218 significantly (Fig. 5E). mRNA levels of the thermogenic gene *Ucp1* decreased
219 substantially, whereas *Fabp4* increased (Fig. 5F). Furthermore, knockout of IL-22R
220 significantly attenuated the increment of multilocular lipid droplets and the decrement

221 of adipocyte size in the subcutaneous fat induced by intermittent fasting (Fig. 5G-H),
222 indicating a reduction in beigeing.

223 To further explore whether IL-22R mediates the effect of ILC3s on beigeing of
224 adipocytes, intestinal ILC3s isolated from intermittent fasting mice were co-cultured
225 with beige adipocytes from subcutaneous SVF of WT or IL-22RKO mice (Fig. 5I-J).
226 Co-culture with ILC3s significantly increased the mRNA levels of thermogenic genes
227 in beige adipocytes derived from WT mice, while demonstrating no effect on beige
228 adipocytes derived from IL-22RKO mice (Fig. 5K). These observations indicate that
229 IL-22R mediates the effect of intestinal ILC3s on beigeing of white adipocytes.

230 5. Profiling of intestinal immune cells in mice fed NCD, HFD or 231 HFD-IF

232 To explore the mechanism by which intermittent fasting promotes the secretion of
233 IL-22 by ILC3s, live $CD45^{+}$ Lineage (CD3, CD5, B220, CD19, Gr1)$^{-}$ cells isolated
234 from the siLP of mice fed NCD, HFD or HFD-IF were subjected for single-cell
235 sequencing (Supplementary Fig. 7A). Following quality controls, we analyzed 7455,
236 4803, 5954 single cells for the NCD, HFD and HFD-IF groups using Seurat-V3.1,
237 respectively. Based on singleR, we identified twenty-five distinct clusters of immune
238 cells (Fig. 6A and Supplementary Fig. 7B), including ILC1s (Cluster 7 and cluster 16),
239 ILC2s (Cluster 2, cluster 12, cluster 13, and cluster 14), ILC3s (cluster 3 and cluster 5),
240 dendritic cells (Cluster 1, cluster 4, cluster 9, cluster 10, cluster 11, cluster 17, cluster
241 18, and cluster 21), eosinophils (Cluster 0 and cluster 6), B cells (Cluster 8 and cluster
242 24), macrophages (Cluster 15, cluster 20, and cluster 23), NKT cells (Cluster 22) and

243 mast cells (Cluster 19). As expected, ILC3s expressed high RNA levels of Il7r (CD127),
244 Rorc, and IL-22 (Fig. 6B, C and Supplementary Fig. 7C, D). ILC3s contain two distinct
245 cell types with highly similar expression profiles: NCR^+ and NCR^-. These ILC3s were
246 distinguished in our analysis as Cluster 5 and Cluster 3 respectively. NCR^- ILC3s
247 (cluster 3) were CCR6 positive and contained lymphoid tissue inducer (LTi) cells (Fig.
248 6B). Interestingly, NCR^- ILC3s were characterized by high levels of vasoactive
249 intestinal peptide receptor 2 (Vipr2) (Fig. 6C), which is critical for the migration and
250 function of ILC3s[29, 32, 33]. The heatmap of cellular composition showed the differences
251 in cell number and percentage among NCD, HFD and HFD IF mice (Supplementary
252 Fig. 8A). The change in ILC3 number was consistent with the flow cytometry results.
253 The percentage of IL-22^+ cells in NCR^+ ILC3s was significantly increased by IF in mice
254 fed HFD (Supplementary Fig. 8B). Moreover, GSEA revealed that HFD-induced
255 decrement of cytokine–cytokine receptor interaction, in which IL-22 is included, was
256 reversed by IF (Supplementary Fig. 8C). Besides, Neuroactive ligand-receptor
257 interaction, in which vipr2 is included, was up-regulated in HFD-IF (Supplementary
258 Fig. 8D). The mRNA levels of *Vipr2* had a tendency to increase in in sorted ILC3s from
259 the small intestine of HFD IF mice compared with that of HFD mice (Supplementary
260 Fig. 8E). Further, gene difference analysis revealed that HFD-induced increase of
261 Zmat4 was significantly attenuated by IF (Fig. 6D, Supplementary Fig. 8F-G).
262 Further, the expression level of Hsp90ab1 in both NCR^- ILC3s and NCR^+ was
263 significantly increased by IF in mice fed HFD (Fig. 6D, Supplementary 10H).
264 Transcription factor analysis using the JASPAR database and TFBS Tools revealed that

265 the expression of *Hsp90ab1* may be regulated by aryl hydrocarbon receptor (AHR) (Fig.
266 6D). AHR is located in the Hsp90:XAP2:p23:Src chaperone protein complex in the
267 cytoplasm without stimulation. Upon binding with the ligand, AhR translocates to the
268 nucleus and heterodimerizes with AhR nuclear translocator (ARNT) to control the
269 transcription of target genes, including AhR repressor (*Ahrr*), *Cyp1a1*, *Cyp1b1* and
270 *Il22*[34]. Consistently, Gene Ontology analysis of the top 20 increased difference genes
271 revealed that aryl hydrocarbon receptor signaling was one of the key pathways affected
272 by intermittent fasting in HFD mice (Fig. 6E-F). Furthermore, the AHR target genes,
273 including *Il22*, *Ahrr*, *Cyp1a1*, *Cyp1b1*, increased significantly in ILC3s sorted from
274 HFD-IF mice compared with HFD mice. These results indicates that intermittent fasting
275 increases the production of IL-22 likely via activation of AhR.

276 6. IF ameliorates the impaired interaction between intestinal 277 myeloid cells and ILC3s

278 Because dendritic cells (DCs) can influence the production of IL-22 by ILC3s, we
279 next analyzed the change in DCs induced by intermittent fasting. IF significantly
280 attenuated the increment of inflammatory factors, such as Ccl4, Ccl17 and Ccl22, of
281 DCs in mice fed HFD (Fig. 7A). Kyoto Encyclopedia of Genes and Genomes (KEGG)
282 analysis of the top 20 differentially expressed genes in cluster 17 revealed that the
283 increase of inflammation-related pathways induced by HFD was obviously attenuated
284 by IF (Fig. 7B-C). These observations indicate that intermittent fasting may ameliorate
285 the inflammatory state of the intestine by decreasing the NOD-like receptor signaling
286 pathway in DCs (Fig. 7B-C).

287 We next analyzed the intestinal cellular communication networks using CellPhone
288 DB analysis based on homologous gene transformation on all immune cells acquired.
289 CellPhone DB ligand–receptor analysis revealed hundreds of immune-to-immune
290 interactions (Supplementary Fig. 9A). Connectome web analysis of siLP immune cells
291 revealed strong interactions among $CD8^+$ dendritic cells (DC) (Cluster 4), $CD127^+$
292 ILC1s (Cluster 16), $DC8^-$ DC-1 (Cluster 9), Macrophages-1 (Cluster 15), $CD8^-$ DC-2
293 (Cluster 1), Macrophages-2 (Cluster 23), $CD8^-$ DC-3 (Cluster 10), $CD8^-$ DC-4 (Cluster
294 11), and $CD8^-$ DC-5 (Cluster 17). Notably, NCR^+ ILC3s strongly interacted with $CD8^+$
295 dendritic cells (DC) (Cluster 4), $CD127^+$ ILC1 s (Cluster 16), $DC8^-$ DC (Cluster 9),
296 macrophages (Cluster 15), $CD8^-$ DC (Cluster 1), macrophages (Cluster 23), $CD8^-$ DC
297 (Cluster 10), $CD8^-$ DC (Cluster 11), and $CD8^-$ DC (Cluster 17). ILC subsets, DCs and
298 macrophages were in the central communication hubs of the healthy small intestine
299 (Supplementary Fig. 9B-C). Analysis of highly expressed interactions uncovered
300 various uncharacterized and validated signaling pathways implicated in intestine
301 homeostasis in mice (Supplementary Fig. 9D). Analysis of the NCD mouse interactome
302 suggests that macrophages (cluster 15) may interact with NCR^+ ILC3s through
303 CD74_COPA, CD74_MIF, CD44_HBEGF, CD44_FGFR2, CCL4_SLC7A1, and
304 IL1B_ADRB2. Similarly, DCs (cluster 9) may interact with NCR^+ILC3s through
305 CD74_COPA, CD74_MIF, IL1B_ADRB2, CD44_HBEGF, and CD44_FGFR2. All
306 these observations indicates that macrophages and DCs play critical roles in the
307 recruitment and maintenance of ILC3s.

308 HFD significantly reduced the interaction between ILC subsets, DCs and

309 macrophages in the small intestine (Fig. 7D and Supplementary Fig. 9B). This reduction
310 was reversed by IF (Fig. 7E and Supplementary Fig. 11B). Analysis of the interactomes
311 in mice fed HFD suggested that IF significantly altered the interacting proteins (Fig.
312 7F-G). To further test this observation, we sorted macrophages and ILC3s from HFD
313 and HFD-IF mice (Supplementary Fig. 10A). As shown in supplementary Fig. 10B-C,
314 *Ccl4* and *Cd74* increased significantly in macrophages, while the receptors expressed
315 on ILC3s remained largely unchanged. Together, these data suggest that IF may
316 promote the production of IL-22 from ILC3s by altering the interactome in intestinal
317 myeloid cells and ILC3s.

318 **Discussion**

319 Our present study demonstrates that intestinal ILC3s are critical for the beigeing of
320 white adipose tissue induced by intermittent fasting. This conclusion is supported by
321 following observations. Firstly, intermittent fasting stimulates the secretion of IL-22 by
322 intestinal ILC3s in either lean mice fed normal chow diet, obese mice fed high-fat diet
323 mice, or mice with metabolic dysfunction induced by HFCD diet. Secondly, a
324 comprehensive set of in vivo and in vitro experiments shows that intermittent fasting
325 promotes adipose tissue beigeing through the intestinal ILC3-IL-22-IL-22R axis.

326 The role of ILC3s in metabolism remains largely unknown. Our studies provide
327 evidence supporting the metabolic benefit of intestinal ILC3s in intermittent fasting.
328 Adoptive transfer of intestinal ILC3s isolated from lean mice was sufficient to improve
329 the metabolic dysfunctions in DIO mice, including increase of white adipose tissue
330 beigeing and glucose tolerance. Interestingly, adoptive transfer of ILC3s significantly

331 increased their number only in intestine. Further, alternate day fasting did not alter the
332 ILC3s in adipose tissue. These observations indicate that ILC3s in intestine rather than
333 in adipose tissue account for the metabolic benefit. OSullivan et al. [16] have reported
334 that ILC3s are negligible in white adipose tissue of either lean or obese mice. Similarly,
335 Sasaki *et al.*[25] have demonstrated that transplanting bone marrow cells from Rag2$^{-/-}$
336 mice (lack of T cells, B cells) into Il2rg$^{-/-}$ Rag2$^{-/-}$ mice (lack of T cells, B cells, ILC cells)
337 could not increase the number of ILC3s in the adipose tissue of recipient mice. However,
338 it is worth of noting that ILC3s have been detected in adipose tissue by other report.
339 Using the marker Lineage^{-}KLRG1^{-}Il-7rα^{+}Thy-1^{+}, ILC3s cells have been reported to
340 account for approximately 20% of lineage^{-}KLRG1^{-}Il-7rα^{+} cells in adipose tissue[31]. In
341 our study, we also detected ILC3s defined as CD127^{+}Lin^{-}RORγt^{+} in adipose tissue.
342 These ILC3s accounted for approximately 10% of CD127^{+}Lin^{-} cells. ILC3s have also
343 been shown to be present in human adipose tissue[35]. Importantly, the proportion and
344 density of ILC3s in white adipose tissue of people with obesity increase relevant to
345 healthy people, and positively correlate with BMI in obese patients. Thus, the existence
346 and function of ILC3s in mouse and human adipose tissue deserve further investigation.
347 Communication between intestine and metabolic organs is currently under active
348 investigation. Our studies identify ILC3s-IL-22-IL-22R as a novel pathway medicating
349 the crosstalk between intestine and adipose tissue. Evidence supporting this conclusion
350 are five folds. (1) Intermittent fasting reverses the reduction of intestinal ILC3s and IL-
351 22 in DIO mice. (2) Adoptive transfer of intestinal ILC3s enhances beigeing of white
352 adipose tissue. (3) Co-culture of intestinal ILC3s with SVF cells increases their

differentiation into beige cells. (4) Exogenous IL-22 mimics the effect of intermittent fasting on beigeing of white adipose tissue. (5) Deficiency of IL-22R blocks the IF-induced beigeing of white adipose tissue. In lines with our observation, a series of recent studies have suggested that cytokines can act directly on adipocytes to regulate thermogenesis. For example, γδ T cells regulate heat production by secreting IL-17[36]. Deficiency of IL-10 increases energy consumption and renders mice resistant to diet-induced obesity[34]. IL-27-IL-27Rα signaling promotes thermogenesis, prevents diet-induced obesity, and improves insulin resistance[37]. IL-33 induces the beigeing of white adipose tissue by activating ILC2s[18]. Our studies extend the effect of cytokines on thermogenesis to IL-22. IL-22 promotes heat production, renders mice resistant to reduction of body temperature induced by cold exposure, and reduces obesity induced by high-fat diet. Together with previous report showing that IL-22 increases the lipolysis of adipocytes, our studies suggest that IL-22 can directly act on adipocytes to alter the adipose tissue homeostasis. IL-22 activates IL-22 receptor, which then regulates the expression of downstream inflammatory factors, tissue repair molecules, chemokines, antimicrobial peptides and other molecules via Jak-1 and Tyk-2 dependent phosphorylation of STAT3. Our studies suggest that IL-22 may promote the expression of downstream thermogenic genes in adipose tissue through IL-22R. Deficiency of IL-22R blocks the up-regulation of thermogenic genes induced by intermittent fasting. SVF cells lacking IL-22R demonstrate no response to the up-regulation of thermogenic genes induced by intestinal ILC3. Thus, our results provide novel evidence supporting the concept that intestinal ILC3s modulate beigeing of adipose tissue via IL-22-IL-22R

375 pathway.

376 The physiological mechanism underlying the secretion of IL-22 by ILC3s remains
377 largely unknown. Our studies reveal the distinct secretion pattern of IL-22 induced by
378 intermittent fasting. Consistently, previous studies have shown that secretion of IL-22
379 by ILC3s changes between active and quiescent periods throughout the day which is
380 regulated by the cycle patterns of food intake[38]. These suggest that secretion of IL-22
381 by ILC3s is altered by feeding rhythm. It is currently unclear how feeding influences
382 the physiological function of ILC3s. Previous studies indicate a mechanism involving
383 neuropeptide vasoactive intestinal peptide (VIP), which is able to stimulate the
384 secretion of IL-22 by ILC3s[29]. Consistently, our single cell RNAseq data also
385 showedthat VIP receptor 2 (VIPR2) is highly expressed in intestinal ILC3s and
386 intermittent fasting activates VIPR2 signaling pathway. Since release of VIP is
387 stimulated by food intake, these observations indicate that VIP-VIPR signaling may
388 coordinate with food intake to drive the production of IL-22. However, conflicting
389 result exists. Studies by Talbot *et al* have shown that VIP inhibits ILC3 secretion of IL-
390 22[32]. Reasons accounting for this difference remains unknown but may be context
391 dependent. Alternatively, we found that intermittent fasting may promote ILC3s
392 secreting IL-22 though activating AhR signaling. Consistently, intermittent fasting has
393 been reported to increase the short-chain fatty acids (SCFAs) acetate and lactate[13],
394 which can lead to activation of AhR and subsequent up-regulation of IL-22
395 production[39]. In addition, feeding may decrease the levels of antimicrobial peptides
396 secreted by epithelial cells, while increasing the expression of lipid-binding proteins[32].

397 Moreover, segmented filamentous bacteria may account for the effect of feeding on the
398 secretion of IL-22 by intestinal ILC3s by periodically attaching to the epithelial
399 surface[38]. These alterations may substantially influence the immune networks in
400 intestine, leading to subsequent change in the secretion of IL-22 by ILC3s. In support
401 of this concept, our single cell RNAseq analysis shows a significant change in the
402 intestinal immune cell network involving dendritic cells, macrophages and ILC3s.
403 Further examination should focus on dissecting the novel molecular mechanism by
404 which intestinal dendritic cells and macrophages interact with ILC3s and its
405 consequence on the IL-22 production.

406 In conclusion, our studies suggest that intermittent fasting can promote the secretion
407 of IL-22 by intestinal ILC3s. IL-22 then directly activates IL-22R on adipocytes,
408 leading to subsequent induction of beigeing of white adipose tissue. Intestinal ILC3s
409 thus may serve as a potential target for the intervention of metabolic disorders.

410 **Materials and Methods**

411 **1. Animals**

412 Four-week-old male C57BL/6 and CD45.1 mice were obtained from Charles River
413 Laboratories (Peking, China). IL-22 receptor knockout mice (IL-22R KO mice, KO-
414 00115) were purchased from BRL Medicine Inc. Mice were handled in accordance with
415 the Guide for the Care and Use of Laboratory Animals prepared by the National
416 Academy of Sciences and published by the National Institutes of Health (NIH
417 publication 86-23, revised 1985). Mice were housed in standard rodent cages and
418 maintained in a regulated environment (21-24°C, humidity at 40-70%, 12:12 h light :

419 dark cycle with lights on at 8:00 AM). A normal chow diet (D12450H; Research Diets)
420 and water were available ad libitum. Obese mice (DIO) were induced with a high-fat
421 diet (60% fat, D12492; Research Diets) for 12 weeks. Eight-week-old C57BL/6 mice
422 received intraperitoneal injection of saline control or IL-22 (R&D, 582-ML) at a dose
423 of 4 μg/kg/day every other day for 6 weeks. All experimental procedures were approved
424 by the Animal Care and Use Committee of Peking University.

425 2. Cell preparation

426 For isolation of small intestine lamina propria cells, small intestines from
427 euthanized mice were emptied of the contents, excised of Peyer's patches, opened
428 longitudinally and cut into 1 cm pieces. The intraepithelial lymphocytes (IELs) were
429 dissociated from the intestine fragments by first shaking the fragments for 20 min at
430 37°C in PBS containing 0.3% BSA, 5 mM EDTA and 1 mM dithiothreitol. Vortex the
431 fragments three times with PBS containing 2 mM EDTA. To isolate lamina propria cells,
432 the remaining fragments were minced and digested at 37°C for 50 min in RPMI 1640
433 medium containing 0.04 mg/mL collagenase IV (Sigma), 0.1 mg/mL
434 deoxyribonuclease (DNase) I (Roche), and 0.5 mg/mL dispase. The digestion
435 suspension was then filtered through a 40 μm cell strainer and centrifuged at 540 g for
436 6 min. Cell pellets were resuspended in PBS containing 2% FBS for further analysis.

437 3. Flow cytometry

438 Single-cell suspensions were preincubated with anti-CD16/32 (clone 2.4G2) for 10
439 min to block the surface Fc receptors. Then, cell-surface molecules were stained with
440 different antibody combinations for 30 min in cell staining buffer. Dead cells were

441 excluded with Fixable Viability Dye eFluor™ 606 (Invitrogen). For intracellular
442 transcription factor staining, the cells were fixed and permeabilized with a Foxp3
443 staining buffer set (eBioscience) according to the manufacturer's protocol.
444 Transcription factor staining usually lasted for more than 4 hours at 4°C. The gate
445 strategy for ILC3s was live lingeage (CD3, CD5, CD19, B220 and Gr-1)$^{-}$
446 CD127^{+}RORγt^{+}. For intracellular cytokine staining, the digested cells were first
447 incubated in RPMI 1640 with 10% FBS and 10 ng/ml recombinant murine IL-7
448 (PeproTech), and stimulated with 50 ng/ml phorbol 12-myristate 13-acetate, 750 ng/ml
449 ionomycin for 3 h and added with 2 μM monensin for the last 2.5 h.

450 Flow cytometry analyses were performed on an LSR Fortessa (BD Biosciences).
451 The flow cytometry data were analyzed with FlowJo software (Tree Star). The antibody
452 used in this study are listed in Supplementary Table 1.

453 4. ILC3s sorting, transfer and co-culture experiment

454 For ILC3s transfer experiment, co-culture experiment and single-cell RNA-Seq,
455 ILCs were collected by FACS. Small intestine lamina propria cells were prepared and
456 stained with surface molecules for 30 min at 4°C followed by sorting on a FACS Aria
457 III cell sorter (BD Biosciences). A gating strategy of live Lineage^{-}CD127^{+}KLRG1^{-}c-
458 Kit^{+} was used to sort the ILC3s.

459 Purification checks were performed after each sort. The cells were suspended in
460 phosphate buffered saline（PBS）and then intravenously injected into HFD mice (200
461 μL PBS/mouse). ILC3s were sorted from 20 WT NCD mice, and sorting for the
462 adoptive transfer was performed six times within 4 weeks from the first injection. The

463 total number of ILC3 injected into HFD mice was 2.4×10^5 cells/mouse/experiment.
464 Mice were placed on an HFD for 16 weeks before ILC3s were transferred. In addition,
465 to confirm that these cells indeed originate from NCD mice, we transferred ILC3s from
466 CD45.1 mice to WT mice and detected the CD45.1 positive cells in recipient mice.

467 5. Single-cell RNA-Seq

468 Single cells were captured via the GemCode Single Cell Platform using the
469 GemCode Gel Bead, Chip and Library Kits (10X Genomics) according to the
470 manufacturer's protocol. Briefly, flow-sorted cells were suspended in PBS containing
471 0.4% BSA and loaded at 6,000 cells per channel. The cells were then partitioned into a
472 GemCode instrument, where individual cells were lysed and mixed with beads carrying
473 unique barcodes in individual oil droplets. The products were subjected to reverse
474 transcription, emulsion breaking, cDNA amplification, shearing, 5′ adaptor and sample
475 index attachment. Libraries were sequenced on a HiSeq 2500 (Illumina).

476 6. Isolation of stromal vascular fraction cells (SVF) and induction 477 of beigeing

478 Isolation of SVF and induction of beigeing were performed as reported[40]. Briefly,
479 subcutaneous white adipose tissue (sWAT) from male C57BL/6 mice was digested with
480 1 mg/mL type 2 collagenase (Sigma–Aldrich) at 37°C for 40 minutes with shaking.
481 Digestion was terminated by complete DMEM/F12 medium containing 10% fetal
482 bovine serum (FBS), 100 units/mL penicillin and 100 units/mL streptomycin
483 (Invitrogen, CA, USA). The cell suspension was centrifuged at 700×g for 10 minutes
484 to separate floating adipocytes from the SVF pellets. The pellets containing the SVF

485 cells were resuspended in complete medium and filtered using a 70 μm diameter filter.
486 The cell suspension was then centrifuged at 700×g for 10 minutes. Cell pellets were
487 resuspended and mixed well and then plated on dishes in complete medium. Cells were
488 grown to 95% confluence in complete medium and then differentiated into beige or
489 white adipocytes as previously described[41]. Briefly, for induction to beige adipocytes,
490 cells were cultured for 2 days with induction medium supplemented with 5 μg/mL
491 insulin, 1 nmol/L T3, 1 μmol/L rosiglitazone, 125 μmol/L indomethacin, 0.5 mmol/L
492 isobutylmethylxanthine (IBMX) and 5 μmol/L dexamethasone. Cells were then
493 cultured in maintenance medium supplemented with 5 μg/ml insulin, 1 nmol/L T3 and
494 1 μmol/L rosiglitazone for 4 days. Fresh media were replaced every 2 days.

495 7. Co-culture experiments

496 To determine the direct effect of ILC3s on beige adipocytes differentiation, SVF
497 were co-cultured with ILC3s using a transwell system (0.4 μm pore size, BD
498 Biosciences). In brief, SVF isolated from adipose tissue were grown in the bottom
499 chamber of the transwell insert in a 12-well plate and induced into beige adipocytes,
500 while sorted ILC3s were seeded in the upper chamber. SVFs cultured alone and SVF
501 cells co-cultured with $CD127^-$ cells were used as controls. After co-culture for 72 h,
502 beige adipocytes in the lower chamber were collected for further detection.

503 8. RNA isolation and qPCR analysis

504 RNA was extracted from cells or adipose tissue using RNATrip (Applied Gene,
505 Beijing, China) and reverse-transcribed into cDNAs with Hifair™ III 1st Strand cDNA
506 Synthesis SuperMix (Yeasen). SYBR Green-based quantitative real-time PCR was

507 performed using the Agilent Aria Mx real-time PCR system. The primer sequences used
508 in this study are listed in Supplementary Table 2.

509 9. Western blot analysis

510 Differentiated SVF cells and sWAT were homogenized using RIPA lysis buffer.
511 Proteins were separated by 10% sodium dodecyl sulfate–polyacrylamide gel
512 electrophoresis and then transferred onto a nitrocellulose (NC) membrane. Membranes
513 were incubated in 5% fat-free milk for 1 hour at room temperature and then incubated
514 with primary antibodies overnight at 4°C. The reaction was detected with IRDye-
515 conjugated secondary antibody and visualized using the Odyssey infrared imaging
516 system (LI-COR Biosciences).

517 10. Histological studies

518 Paraffin-embedded sWAT sections were stained with hematoxylin-eosin (H&E).
519 Images were scanned using a NanoZoomer-SQ (Hamamatsu).

520 11. Oil red O staining

521 Cells were washed with PBS for three times, and then fixed with 4%
522 paraformaldehyde for 30 minutes. Next, the cells were stained with oil red O for 60
523 minutes, and washed with PBS for 5 minutes. Cells were then stained with hematoxylin
524 for 5 seconds and washed with PBS. The dyed cells were photographed under the
525 microscope (Leica, Germany).

526 12. Enzyme-linked immunosorbent assay

527 Levels of IL-22 were measured by double-antibody sandwich enzyme-linked
528 immunosorbent assays (ELISAs) (M2200; R&D Systems). Briefly, 100 μL of Assay

529 Diluent were added to each well. 50 uL of blood samples and standards were added and
530 incubated at room temperature for 2 hours. After washing, conjugates were added and
531 incubated for 2 hours. After washing, the substrate solution was added and incubated
532 for 30 minutes and washed. And stop solution were added finally. Optical density (OD)
533 values were measured using a microplate reader (Bio-Rad, Hercules, CA, USA).

534 **13. OGTT and ITT**

535 Oral Glucose tolerance tests (OGTT) and insulin tolerance tests (ITT) were
536 performed after 16 or 6 hours of fasting, respectively. Mice were given with 3 g/kg
537 glucose by gavage or injected intraperitoneally with 0.75 U/kg insulin. Blood samples
538 were collected from the tail vain at 0, 15, 30, 60, 90 and 120 min after glucose or insulin
539 treatment. Blood glucose levels were measured using a glucometer (Roche, Basel, CH).

540 **14. Cold exposure**

541 Mice were placed in a 4°C cold room for 6 hours. The rectal temperature was
542 measured every hour during the cold challenge with a rectal probe (Braintree Scientific,
543 Braintree, MA).

544 **15. Statistical analysis**

545 Data were analyzed by GraphPad Prism software v.8.0 and presented as the mean
546 ±s.e.m. The Shapiro–Wilk normality test was used to determine the normal distribution
547 of samples. Unpaired Student's *t* test (normal distribution) or Mann–Whitney U-tests
548 (non-normal distribution) was used to analyze data between two groups and one-way
549 ANOVA followed by Bonferroni's multiple-comparisons test (normal distribution) or
550 Kruskal–Wallis test (non-normal distribution) was used for three or more groups. The

sample sizes were determined by power analysis using StatMate v.2.0. No data were excluded during the data analysis.

References

[1] Liu B, Du Y, Wu Y, Snetselaar L G, Wallace R B, Bao W. Trends in obesity and adiposity measures by race or ethnicity among adults in the united states 2011-18: Population based study. Bmj. 2021, 372: n365

[2] Colman R J, Anderson R M, Johnson S C, Kastman E K, Kosmatka K J, Beasley T M, Allison D B, Cruzen C, Simmons H A, Kemnitz J W, Weindruch R. Caloric restriction delays disease onset and mortality in rhesus monkeys. Science (New York, N.Y.). 2009, 325(5937): 201-204

[3] Mattison J A, Roth G S, Beasley T M, Tilmont E M, Handy A M, Herbert R L, Longo D L, Allison D B, Young J E, Bryant M, Barnard D, Ward W F, Qi W, Ingram D K, de Cabo R. Impact of caloric restriction on health and survival in rhesus monkeys from the nia study. Nature. 2012, 489(7415): 318-321

[4] Mattison J A, Colman R J, Beasley T M, Allison D B, Kemnitz J W, Roth G S, Ingram D K, Weindruch R, de Cabo R, Anderson R M. Caloric restriction improves health and survival of rhesus monkeys. Nature Communications. 2017, 8: 14063

[5] Ulgherait M, Midoun A M, Park S J, Gatto J A, Tener S J, Siewert J, Klickstein N, Canman J C, Ja W W, Shirasu-Hiza M. Circadian autophagy drives iTRF-mediated longevity. Nature. 2021, 598(7880): 353-358

[6] Stekovic S, Hofer S J, Tripolt N, Aon M A, Royer P, Pein L, Stadler J T, Pendl T,

Prietl B, Url J, Schroeder S, Tadic J, Eisenberg T, Magnes C, Stumpe M, Zuegner E, Bordag N, Riedl R, Schmidt A, Kolesnik E, Verheyen N, Springer A, Madl T, Sinner F, de Cabo R, Kroemer G, Obermayer-Pietsch B, Dengjel J, Sourij H, Pieber T R, Madeo F. Alternate day fasting improves physiological and molecular markers of aging in healthy, non-obese humans. Cell Metabolism. 2019, 30(3): 878-881

[7] de Cabo R, Mattson M P. Effects of intermittent fasting on health, aging, and disease. New England Journal of Medicine. 2019, 381(26): 2541-2551

[8] Hepler C, Weidemann B J, Waldeck N J, Marcheva B, Cedernaes J, Thorne A K, Kobayashi Y, Nozawa R, Newman M V, Gao P, Shao M, Ramsey K M, Gupta R K, Bass J. Time-restricted feeding mitigates obesity through adipocyte thermogenesis. Science. 2022, 378(6617): 276-284

[9] Mattson M P, Moehl K, Ghena N, Schmaedick M, Cheng A. Intermittent metabolic switching, neuroplasticity and brain health. Nature Reviews. Neuroscience. 2018, 19(2): 63-80

[10] Liu Y, Cheng A, Li Y-J, Yang Y, Kishimoto Y, Zhang S, Wang Y, Wan R, Raefsky S M, Lu D, Saito T, Saido T, Zhu J, Wu L-J, Mattson M P. Sirt3 mediates hippocampal synaptic adaptations to intermittent fasting and ameliorates deficits in app mutant mice. Nature Communications. 2019, 10(1): 1886

[11] Mattson M P, Arumugam T V. Hallmarks of brain aging: Adaptive and pathological modification by metabolic states. Cell Metabolism. 2018, 27(6): 1176-1199

[12] Kim K-H, Kim Y H, Son J E, Lee J H, Kim S, Choe M S, Moon J H, Zhong J, Fu K, Lenglin F, Yoo J-A, Bilan P J, Klip A, Nagy A, Kim J-R, Park J G, Hussein S M,

595 Doh K-O, Hui C-C, Sung H-K. Intermittent fasting promotes adipose thermogenesis
596 and metabolic homeostasis via VEGF-mediated alternative activation of
597 macrophage. Cell Research. 2017, 27(11): 1309-1326
598 [13] Li G, Xie C, Lu S, Nichols R G, Tian Y, Li L, Patel D, Ma Y, Brocker C N, Yan T,
599 Krausz K W, Xiang R, Gavrilova O, Patterson A D, Gonzalez F J. Intermittent
600 fasting promotes white adipose browning and decreases obesity by shaping the
601 gut microbiota. Cell Metabolism. 2017, 26(4): 672-685.e674
602 [14] Gasteiger G, Fan X, Dikiy S, Lee S Y, Rudensky A Y. Tissue residency of innate
603 lymphoid cells in lymphoid and nonlymphoid organs. Science (New York, N.Y.).
604 2015, 350(6263): 981-985
605 [15] Vivier E, Artis D, Colonna M, Diefenbach A, Di Santo J P, Eberl G, Koyasu S,
606 Locksley R M, McKenzie A N J, Mebius R E, Powrie F, Spits H. Innate lymphoid
607 cells: 10 years on. Cell. 2018, 174(5): 1054-1066
608 [16] O'Sullivan T E, Rapp M, Fan X, Weizman O-E, Bhardwaj P, Adams N M, Walzer
609 T, Dannenberg A J, Sun J C. Adipose-resident group 1 innate lymphoid cells
610 promote obesity-associated insulin resistance. Immunity. 2016, 45(2): 428-441
611 [17] Wang H, Shen L, Sun X, Liu F, Feng W, Jiang C, Chu X, Ye X, Jiang C, Wang Y,
612 Zhang P, Zang M, Zhu D, Bi Y. Adipose group 1 innate lymphoid cells promote
613 adipose tissue fibrosis and diabetes in obesity. Nat Commun. 2019, 10(1): 3254
614 [18] Brestoff J R, Kim B S, Saenz S A, Stine R R, Monticelli L A, Sonnenberg G F,
615 Thome J J, Farber D L, Lutfy K, Seale P, Artis D. Group 2 innate lymphoid cells
616 promote beiging of white adipose tissue and limit obesity. Nature. 2015, 519(7542):

617 242-246

618 [19] Lee M W, Odegaard J I, Mukundan L, Qiu Y, Molofsky A B, Nussbaum J C, Yun
619 K, Locksley R M, Chawla A. Activated type 2 innate lymphoid cells regulate beige
620 fat biogenesis. Cell. 2015, 160(1-2): 74-87

621 [20] Wang L, Luo Y, Luo L, Wu D, Ding X, Zheng H, Wu H, Liu B, Yang X, Silva F,
622 Wang C, Zhang X, Zheng X, Chen J, Brigman J, Mandell M, Zhou Z, Liu F, Yang
623 X O, Liu M. Adiponectin restrains ILC2 activation by ampk-mediated feedback
624 inhibition of IL-33 signaling. J Exp Med. 2021, 218(2):

625 [21] Sanos S L, Bui V L, Mortha A, Oberle K, Heners C, Johner C, Diefenbach A.
626 Rorgammat and commensal microflora are required for the differentiation of
627 mucosal interleukin 22-producing NKp46^{+} cells. Nature Immunology. 2009, 10(1):
628 83-91

629 [22] Wang X, Ota N, Manzanillo P, Kates L, Zavala-Solorio J, Eidenschenk C, Zhang
630 J, Lesch J, Lee W P, Ross J, Diehl L, van Bruggen N, Kolumam G, Ouyang W.
631 Interleukin-22 alleviates metabolic disorders and restores mucosal immunity in
632 diabetes. Nature. 2014, 514(7521): 237-241

633 [23] Hasnain S Z, Borg D J, Harcourt B E, Tong H, Sheng Y H, Ng C P, Das I, Wang
634 R, Chen A C H, Loudovaris T, Kay T W, Thomas H E, Whitehead J P, Forbes J M,
635 Prins J B, McGuckin M A. Glycemic control in diabetes is restored by therapeutic
636 manipulation of cytokines that regulate beta cell stress. Nature Medicine. 2014,
637 20(12): 1417-1426

638 [24] Qi X, Yun C, Sun L, Xia J, Wu Q, Wang Y, Wang L, Zhang Y, Liang X, Wang L,

639 Gonzalez F J, Patterson A D, Liu H, Mu L, Zhou Z, Zhao Y, Li R, Liu P, Zhong C,
640 Pang Y, Jiang C, Qiao J. Gut microbiota–bile acid–interleukin-22 axis orchestrates
641 polycystic ovary syndrome. Nature Medicine. 2019, 25(8): 1225-1233
642 [25] Sasaki T, Moro K, Kubota T, Kubota N, Kato T, Ohno H, Nakae S, Saito H, Koyasu
643 S. Innate lymphoid cells in the induction of obesity. Cell Reports. 2019, 28(1): 202-
644 217.e207
645 [26] Upadhyay V, Poroyko V, Kim T J, Devkota S, Fu S, Liu D, Tumanov A V, Koroleva
646 E P, Deng L, Nagler C, Chang E B, Tang H, Fu Y X. Lymphotoxin regulates
647 commensal responses to enable diet-induced obesity. Nat Immunol. 2012, 13(10):
648 947-953
649 [27] Wang Y, Kuang Z, Yu X, Ruhn K A, Kubo M, Hooper L V. The intestinal
650 microbiota regulates body composition through nfil3 and the circadian clock.
651 Science. 2017, 357(6354): 912-916
652 [28] Kawano Y, Edwards M, Huang Y, Bilate A M, Araujo L P, Tanoue T, Atarashi K,
653 Ladinsky M S, Reiner S L, Wang H H, Mucida D, Honda K, Ivanov, II. Microbiota
654 imbalance induced by dietary sugar disrupts immune-mediated protection from
655 metabolic syndrome. Cell. 2022, 185(19): 3501-3519.e3520
656 [29] Seillet C, Luong K, Tellier J, Jacquelot N, Shen R D, Hickey P, Wimmer V C,
657 Whitehead L, Rogers K, Smyth G K, Garnham A L, Ritchie M E, Belz G T. The
658 neuropeptide vip confers anticipatory mucosal immunity by regulating ILC3
659 activity. Nature Immunology. 2020, 21(2): 168-177
660 [30] Victor A R, Nalin A P, Dong W, McClory S, Wei M, Mao C, Kladney R D, Youssef

661 Y, Chan W K, Briercheck E L, Hughes T, Scoville S D, Pitarresi J R, Chen C, Manz
662 S, Wu L C, Zhang J, Ostrowski M C, Freud A G, Leone G W, Caligiuri M A, Yu J.
663 Il-18 drives ILC3 proliferation and promotes IL-22 production via nf-κb. J Immunol.
664 2017, 199(7): 2333-2342
665 [31] Zou J, Chassaing B, Singh V, Pellizzon M, Ricci M, Fythe M D, Kumar M V,
666 Gewirtz A T. Fiber-mediated nourishment of gut microbiota protects against diet-
667 induced obesity by restoring IL-22-mediated colonic health. Cell Host Microbe.
668 2018, 23(1): 41-53.e44
669 [32] Talbot J, Hahn P, Kroehling L, Nguyen H, Li D, Littman D R. Feeding-dependent
670 vip neuron-ILC3 circuit regulates the intestinal barrier. Nature. 2020, 579(7800):
671 575-580
672 [33] Yu H B, Yang H, Allaire J M, Ma C, Graef F A, Mortha A, Liang Q, Bosman E S,
673 Reid G S, Waschek J A, Osborne L C, Sokol H, Vallance B A, Jacobson K.
674 Vasoactive intestinal peptide promotes host defense against enteric pathogens by
675 modulating the recruitment of group 3 innate lymphoid cells. Proceedings of the
676 National Academy of Sciences of the United States of America. 2021, 118(41):
677 e2106634118
678 [34] Stockinger B, Di Meglio P, Gialitakis M, Duarte J H. The aryl hydrocarbon
679 receptor: Multitasking in the immune system. Annu Rev Immunol. 2014, 32: 403-
680 432
681 [35] Hildreth A D, Ma F, Wong Y Y, Sun R, Pellegrini M, OSullivan T E. Single-cell
682 sequencing of human white adipose tissue identifies new cell states in health and

683 obesity. Nature Immunology. 2021, 22(5): 639-653

684 [36] Hu B, Jin C, Zeng X, Resch J M, Jedrychowski M P, Yang Z, Desai B N, Banks A
685 S, Lowell B B, Mathis D, Spiegelman B M. γδ T cells and adipocyte il-17rc control
686 fat innervation and thermogenesis. Nature. 2020, 578(7796): 610-614

687 [37] Wang Q, Li D, Cao G, Shi Q, Zhu J, Zhang M, Cheng H, Wen Q, Xu H, Zhu L,
688 Zhang H, Perry R J, Spadaro O, Yang Y, He S, Chen Y, Wang B, Li G, Liu Z, Yang
689 C, Wu X, Zhou L, Zhou Q, Ju Z, Lu H, Xin Y, Yang X, Wang C, Liu Y, Shulman G
690 I, Dixit V D, Lu L, Yang H, Flavell R A, Yin Z. Il-27 signalling promotes adipocyte
691 thermogenesis and energy expenditure. Nature. 2021, 600(7888): 314-318

692 [38] Brooks J F, Behrendt C L, Ruhn K A, Lee S, Raj P, Takahashi J S, Hooper L V. The
693 microbiota coordinates diurnal rhythms in innate immunity with the circadian clock.
694 Cell. 2021, 184(16): 4154–4167.e4112

695 [39] Yang W, Yu T, Huang X, Bilotta A J, Xu L, Lu Y, Sun J, Pan F, Zhou J, Zhang W,
696 Yao S, Maynard C L, Singh N, Dann S M, Liu Z, Cong Y. Intestinal microbiota-
697 derived short-chain fatty acids regulation of immune cell IL-22 production and gut
698 immunity. Nat Commun. 2020, 11(1): 4457

699 [40] Aune U L, Ruiz L, Kajimura S. Isolation and differentiation of stromal vascular
700 cells to beige/brite cells. J Vis Exp. 2013, (73): 50191

701 [41] Seale P, Conroe H M, Estall J, Kajimura S, Frontini A, Ishibashi J, Cohen P, Cinti
702 S, Spiegelman B M. Prdm16 determines the thermogenic program of subcutaneous
703 white adipose tissue in mice. The Journal of Clinical Investigation. 2011, 121(1):
704 96-105

Figure and Figure Legends

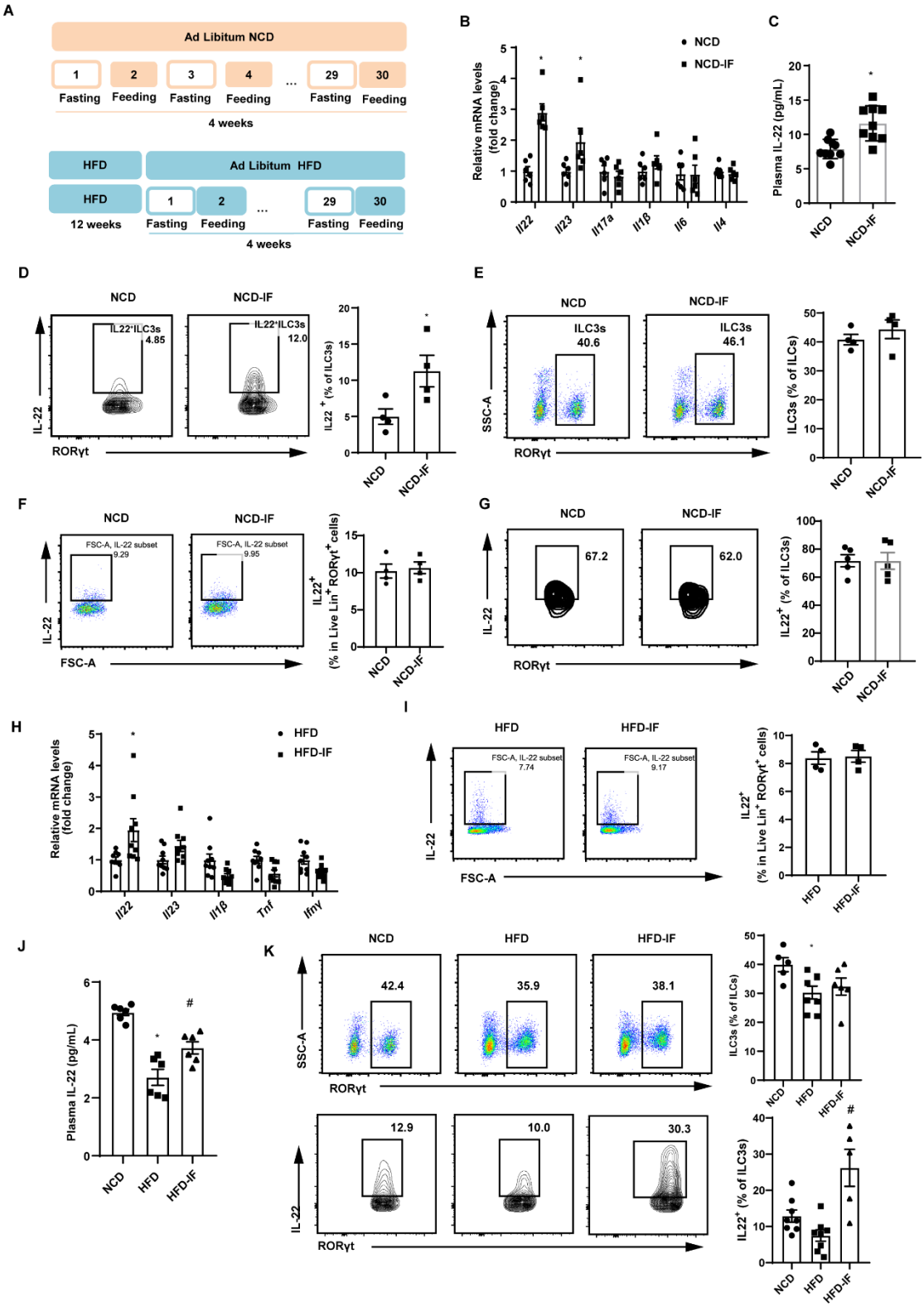

Fig. 1. Intermittent fasting enhances IL-22 production by intestinal ILC3s.

A Schematic illustration of the alternate day fasting regimen. NCD, normal chow diet.

709 HFD, high-fat diet. We applied alternate-day fasting to mice fed normal chow diet
710 (NCD-IF group) or high-fat diet (HFD-IF group). The control groups were at free access
711 to NCD (NCD group) or HFD (HFD group). n =9 for each group.
712 B mRNA expression levels of cytokine genes in the small intestine of NCD and NCD
713 intermittent fasting (NCD-IF) mice. qPCR results were normalized to β-actin. n=6 for
714 each group.
715 C Protein levels of IL-22 in plasma of NCD and NCD intermittent fasting (NCD-IF)
716 mice. n=9 for each group.
717 D Flow cytometric analysis of IL-22^{+} cells in live CD127^{+} lineage^{-} RORγt^{+} ILC3s from
718 the small intestine lamina propria (siLP) of NCD and NCD intermittent fasting (NCD-
719 IF) mice. Four independent experiments were performed with similar results. n=4.
720 E Flow cytometric analysis of RORγt^{+} ILC3s in live CD127^{+} lineage^{-} ILCs in the small
721 intestine lamina propria of NCD and NCD intermittent fasting (NCD-IF) mice. n=4.
722 F Flow cytometric analysis of IL-22^{+} cells in Live Lineage^{+} RORγt^{+} cells in the small
723 intestine lamina propria of mice fed NCD with or without intermittent fasting. n=4.
724 G Flow cytometric analysis of IL-22^{+} cells in CD90.2^{+} Lineage^{-} RORγt^{+} ILC3s from
725 the SVF cells of sWAT in mice fed NCD with or without intermittent fasting. n=5.
726 H mRNA expression levels of cytokine genes in the small intestine of mice fed HFD
727 with or without intermittent fasting. qPCR results were normalized to β–actin. n=9.
728 I Flow cytometric analysis of IL-22^{+} cells in Live Lineage^{+} RORγt^{+} cells in the small
729 intestine lamina propria of mice fed HFD with or without intermittent fasting. n=4.
730 J Levels of IL-22 in plasma of NCD mice, HFD mice and HFD-IF mice. n=6.

731 K Flow cytometric analysis of RORγt^{+} ILC3s in live CD127^{+} lineage^{-} ILCs and flow
732 cytometric analysis of IL-22^{+} cells in live CD127^{+} lineage^{-} RORγt^{+} ILC3s from the
733 small intestine lamina propria of NCD mice, HFD mice and HFD-IF mice. n=5-8. * vs
734 NCD, # vs HFD, P<0.05.
735 All data represent the mean ± s.e.m. Statistical significance was determined by unpaired
736 two-tailed Student's *t* test (A-I) or one-way ANOVA with Bonferroni's multiple-
737 comparisons test (J-K). NCD, normal chow diet. HFD, high-fat diet. NCD-IF, normal
738 chow diet with intermittent fasting. HFD-IF, high-fat diet with intermittent fasting.

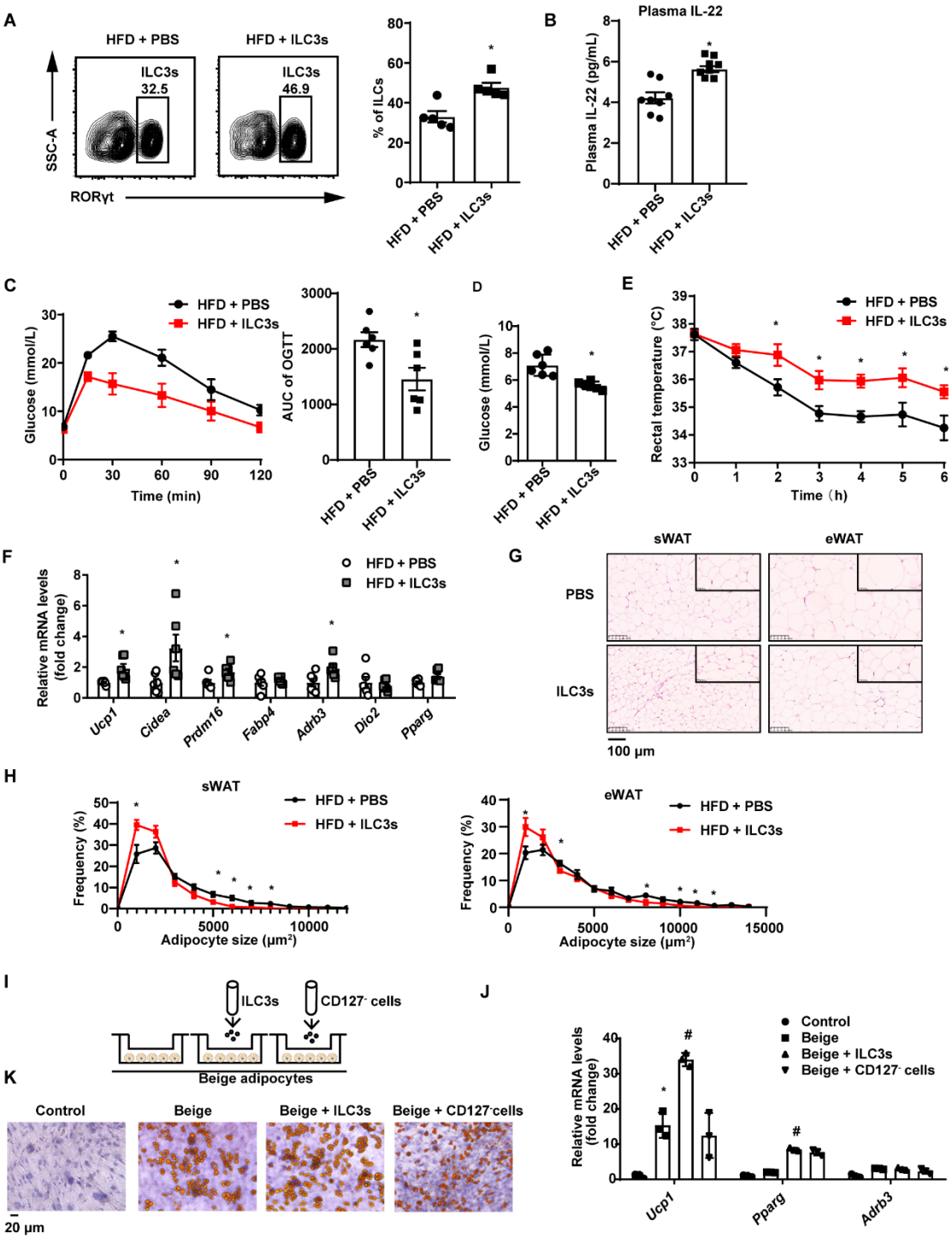

Fig. 2. ILC3s promote beigeing of white adipose tissue.

6 weeks old male C57BL/6J SPF wild type mice were fed with HFD for 16 weeks and then injected with ILC3s (HFD + ILC3s group) or PBS (HFD + PBS group) intravenously six times in a month. n=8 for each group.

A. Flow cytometric analysis of RORγt^{+} ILC3s in live CD127^{+} lineage^{-} ILCs from the

745 siLP of mice transferred with PBS or ILC3s. The proportion of ILC3s in ILCs was
746 shown in the histogram. n=5 for each group.
747 B. Levels of IL-22 in plasma. n=8 for each group.
748 C. Oral glucose tolerance test (OGTT) and area under the curve (AUC). n=6 mice/group.
749 D. Random blood glucose. n=6 mice/group.
750 E. Rectal temperature of HFD mice transferred with PBS or ILC3s during a 6 h cold
751 challenge (4 °C). n=6 mice/group.
752 F. qPCR analysis of thermogenic genes in sWAT. n=6 mice/group.
753 G. Representative images of hematoxylin-and-eosin-stained sections of sWAT, eWAT
754 and BAT from HFD mice transferred with ILC3s or control (n=5).
755 H. Distribution and average adipocyte size of sWAT and eWAT were shown (n=5).
756 I. Schematic depicting the coculture of ILC3s with SVF-derived beige adipocytes.
757 J. qPCR analysis of thermogenic genes in SVF-derived cells. * indicates P<0.05 vs
758 Control, # denotes P<0.05vs Beige. n=3.
759 K. Oil red O staining of adipocytes after coculture with ILC3s or $CD127^-$ cells.
760 All data represent the means ± SEM. Statistical significance was determined by
761 unpaired two-tailed Student's *t* test (A-H), one-way ANOVA with Bonferroni's
762 multiple-comparisons test (J).

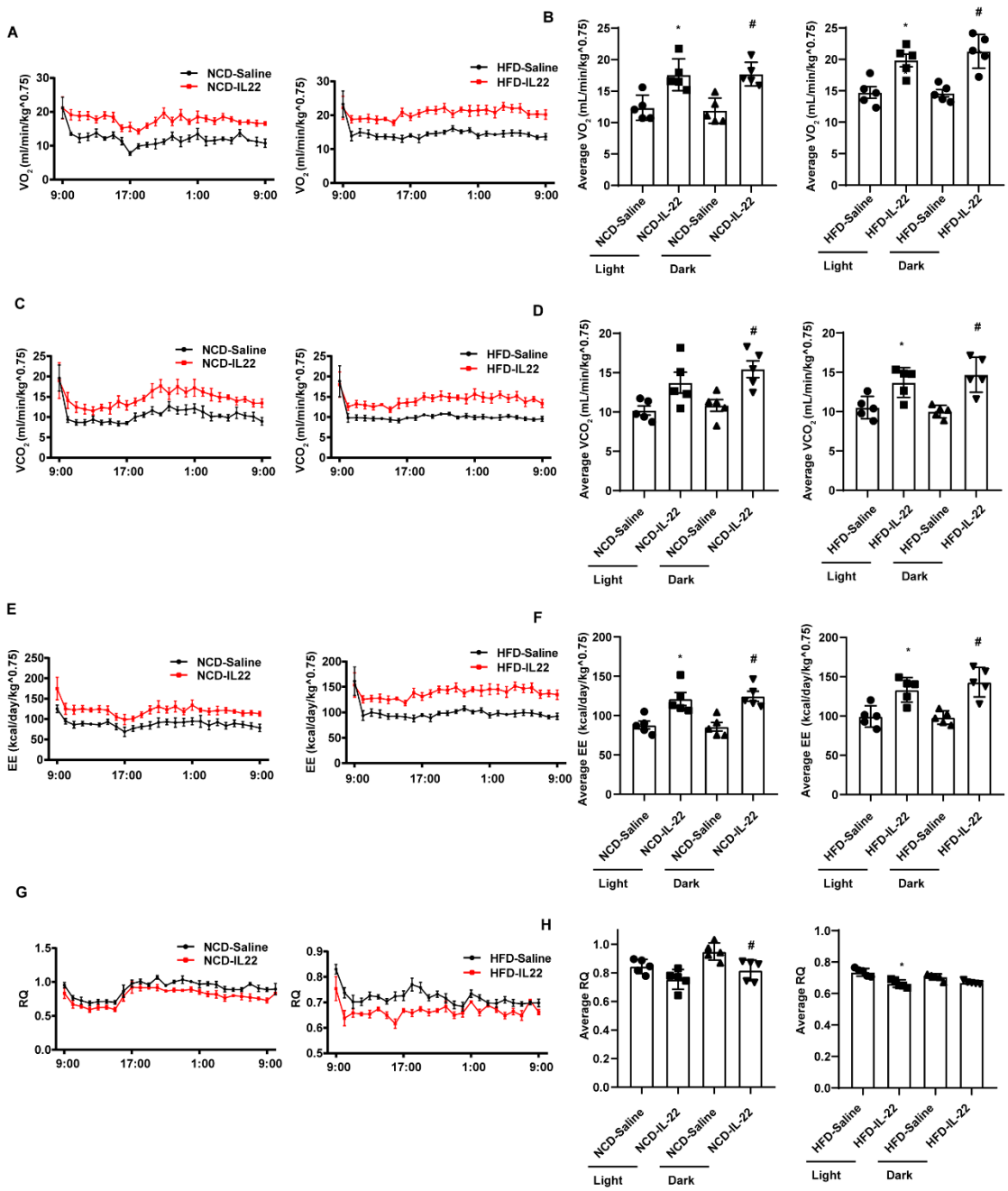

Fig.3. IL-22 promotes energy expenditure.

6 weeks old male C57BL/6J SPF wild type mice were fed NCD or HFD for 12 weeks and then divided into four groups (NCD-Saline, NCD-IL-22, HFD-Saline, HFD-IL-22). Mice were intraperitoneally injected with 4 μg/kg IL-22 every other day for six weeks. The control groups were injected with saline.

A VO_2 of mice fed NCD or HFD.

770 B. Average VO_2 at light and dark respectively.

771 C. VCO_2 of mice fed NCD or HFD.

772 D. Average VCO_2 at light and dark respectively.

773 E. Energy expenditure of mice fed NCD or HFD.

774 F. Average energy expenditure at light and dark respectively.

775 G. Respiratory quotient (RQ) of mice fed NCD or HFD

776 H. Average respiratory quotient at light and dark respectively.

777 * indicates $P<0.05$ vs NCD-Saline or HFD-Saline at light. # indicates $P<0.05$ vs NCD-

778 Saline or HFD-Saline at dark. n=5.

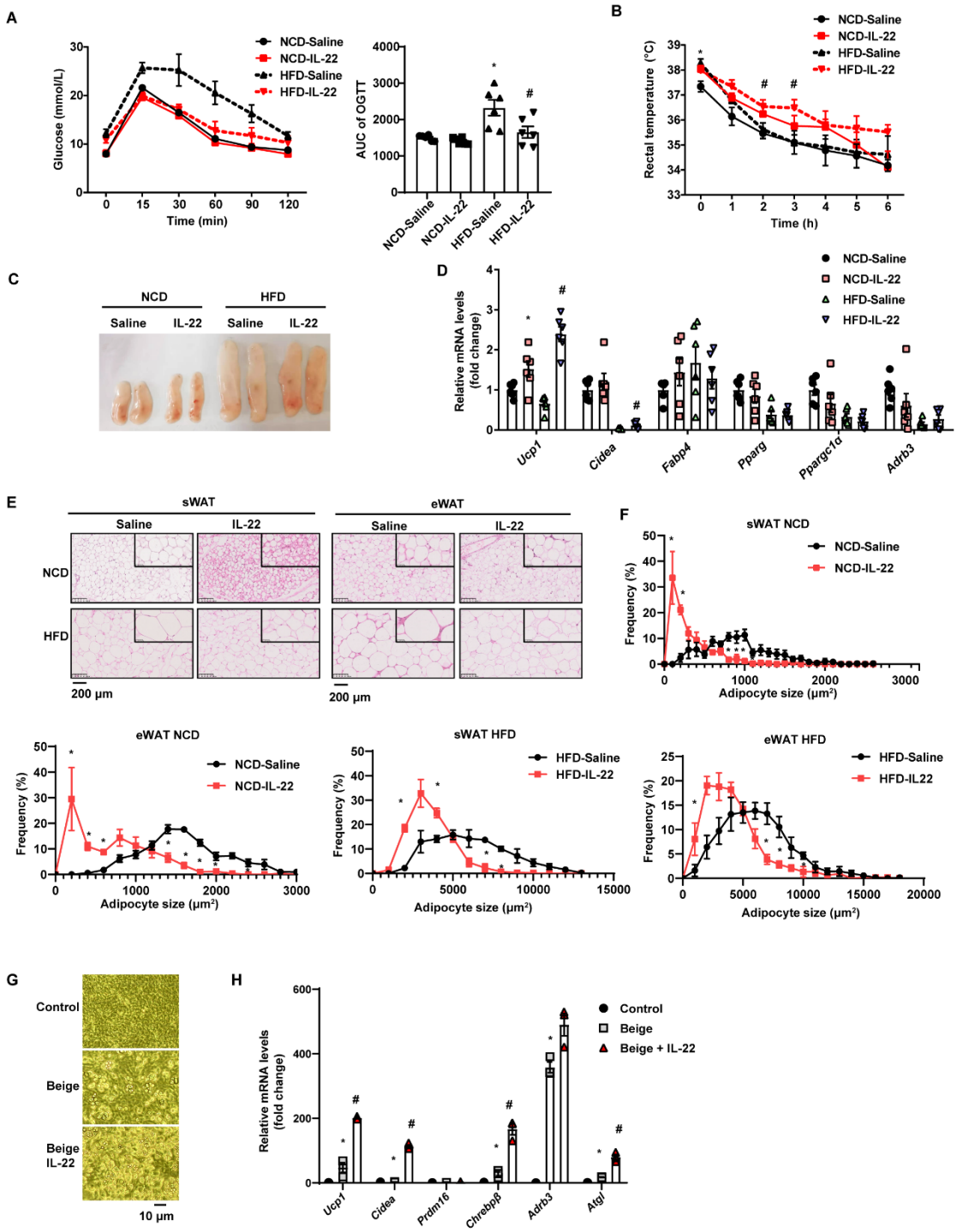

Fig. 4. IL-22 promotes beigeing of white adipose tissue.

6 weeks old male C57BL/6J SPF wild type mice were fed NCD or HFD for 12 weeks and then divided into four groups (NCD-Saline, NCD-IL-22, HFD-Saline, HFD-IL-22). Mice were intraperitoneally injected with 4 μg/kg IL-22 every other day for 6 weeks. The saline group was injected with saline. n=6 mice/group.

785 A. Oral glucose tolerance test (OGTT) and area under the curve (AUC). n=6 mice/group.
786 * indicates P<0.05 vs NCD-Saline; # denotes P<0.05 vs HFD-Saline.
787 B. Rectal temperature of mice during a 6 h cold challenge (4 °C). n=6. * indicates
788 P<0.05 vs NCD-Saline; # denotes P<0.05 vs HFD-Saline.
789 C. Representative image of sWAT of the four groups, NCD-Saline, NCD-IL-22, HFD-
790 Saline, HFD-IL-22.
791 D. qPCR analysis of thermogenic genes of sWAT. n=6 mice/group. * indicates P<0.05
792 vs NCD-Saline; # denotes P<0.05 vs HFD-Saline.
793 E. Representative images of hematoxylin-and-eosin-stained sections of sWAT and
794 eWAT (n=5 for each group).
795 F. The distribution and average adipocyte size of sWAT and eWAT were determined by
796 ImageJ.
797 G. Phase-contrast microscopic images of SVF cells
798 H. qPCR analysis of thermogenic genes in SVF cells. n=3. # denotes P<0.05 vs Beige.
799 All data represent the mean ± s.e.m. Statistical significance was determined by one-
800 way ANOVA with Bonferroni's multiple-comparisons test (A-D, H) or two-tailed
801 Student's *t* test (F). sWAT, subcutaneous white adipose tissue; eWAT, epididymal white
802 adipose tissue.

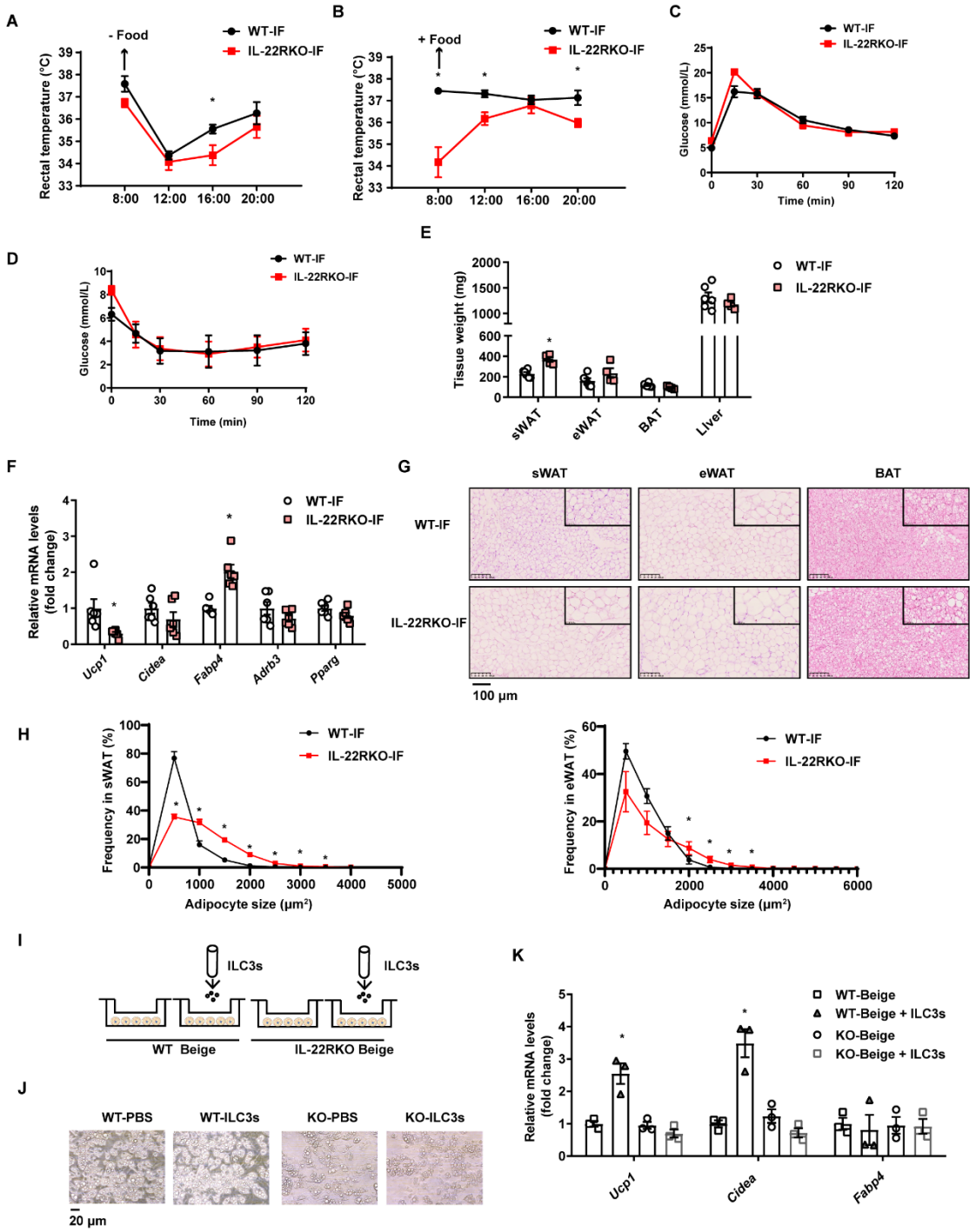

Fig. 5. IL-22RKO blocks white adipose tissue beigeing induced by intermittent fasting.

8 weeks old IL-22RKO and wild type mice were subjected to alternate day fasting for 30 days. n =6 mice per group.

A. Rectal temperature of mice at room temperature during the fasting day. n=6 per

809 group.

810 B. Rectal temperature of mice at room temperature during the fed day. n=6 per group.

811 C. Oral glucose tolerance test (OGTT) of WT-IF mice and IL-22RKO-IF mice. n=6 per

812 group.

813 D. Insulin tolerance test (ITT) of WT-IF mice and IL-22RKO-IF mice. n=6 per group.

814 E. Tissue weight of sWAT, eWAT, BAT, and liver from WT-IF and IL-22RKO-IF mice.

815 n=6 mice/group.

816 F. qPCR analysis of thermogenic genes in sWAT from WT-IF and IL-22RKO-IF mice.

817 n=6 mice/group.

818 G. Representative images of hematoxylin-and-eosin-stained sections of sWAT, eWAT

819 and BAT (n=5 for each group).

820 H. The distribution and average adipocyte size of sWAT and eWAT were determined by

821 ImageJ.

822 I. Schematic depicting the co-culture of ILC3s with SVF-induced beige adipocytes

823 from WT or IL-22RKO mice. n=3. Experiments were repeated 3 times.

824 J. Phase contrast microscopy images of beige adipocytes differentiated from SVF cells

825 cocultured with or without ILC3s. Shown are representatives from one experiment.

826 K. qPCR analysis of thermogenic genes in SVF-derived cells co-cultured with or

827 without ILC3s. n=3.

828 All data represent the means ± SEM. Statistical significance was determined by

829 unpaired two-tailed Student's *t* test (A-H) or one-way ANOVA with Bonferroni's

830 multiple-comparisons test (K).

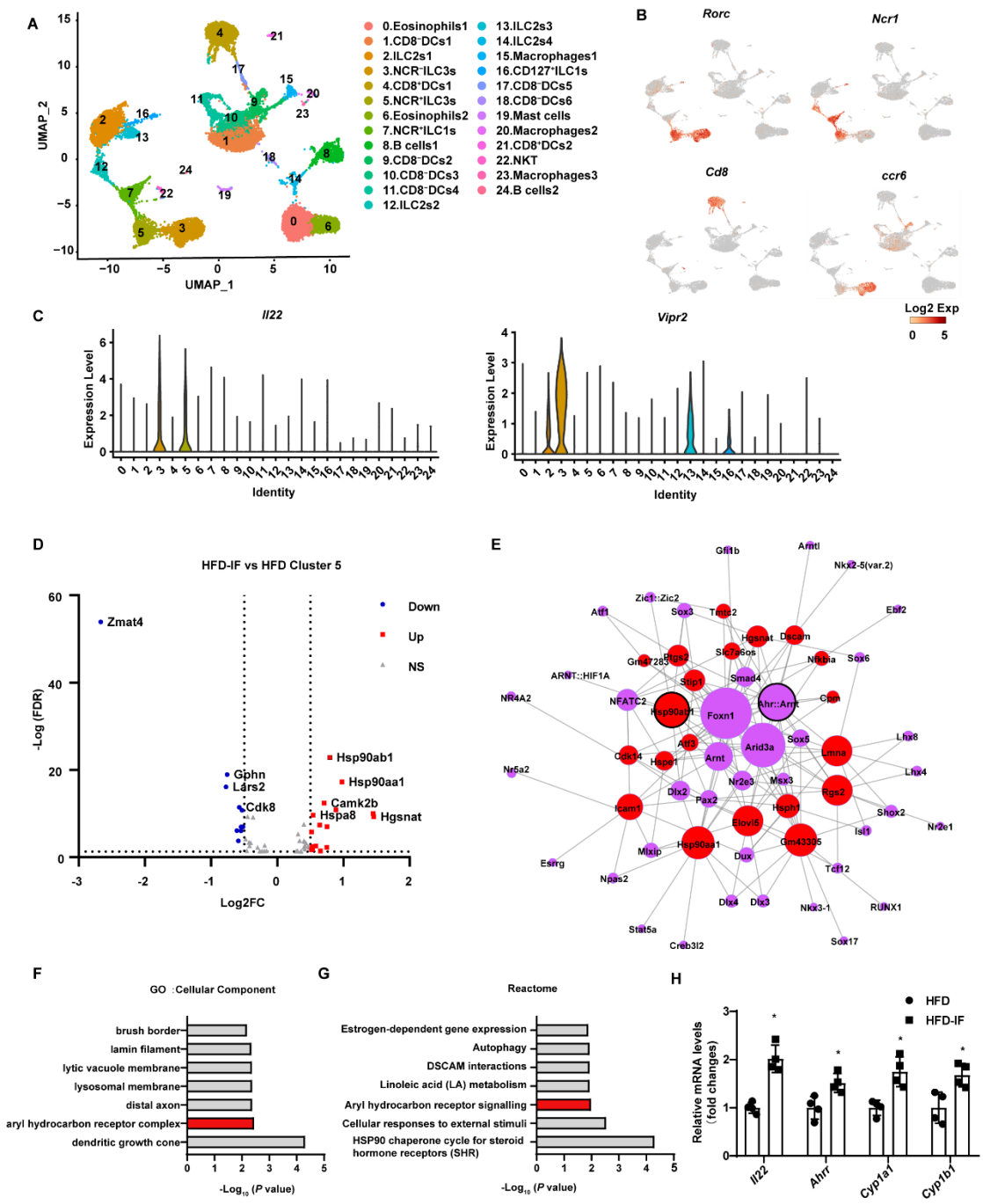

Fig. 6. Profiling of intestinal immune cells derived from mice fed NCD, HFD and HFD-IF.

Live CD45+ Lineage -Cells sorted from mice fed normal chow diet (NCD group), high-fat diet (HFD- group), high-fat diet with alternate day fasting (HFD-IF group) were analyzed using single cell sequencing.

A. Cell subsets in the small intestine lamina propria CD45^{+} Lineage^{-} immune cell atlas.

838 Two-dimensional (2D) representation of cell profiles (dots) from the small intestine
839 lamina propria, colored and numbered by cluster membership.
840 B-C. UMAP feature plots (B) and violin plots (C) showing RNA expression of cluster
841 markers for the indicated cell populations. UMAP feature plots are based on the UMAP
842 shown in Figure 6A.
843 D. The volcano plot of differentially expressed genes in Cluster 5 (NCR^+ ILC3s). The
844 red dots represent upregulated genes in HFD-IF group compared with HFD group,
845 while the blue dots represent downregulated genes in HFD-IF group compared with
846 HFD group. Hsp90ab1 is one of the notably upregulated genes.
847 E. Transcription factor prediction using the Jaspar database and TFBS tools. Red dots
848 represent differentially expressed genes, purple dots represent transcription factors, and
849 larger nodes represent more nodes connected to them.
850 F. Gene ontology (GO) of the top 20 differentially expressed genes in Cluster 5. The
851 cellular component up GO terms in HFD-IF group compared with HFD group.
852 G. The reactome up terms of Cluster 5 top 20 differential genes in HFD-IF group
853 compared with HFD group.
854 H. qPCR analysis of AHR target genes in ILC3s sorted from HFD and HFD-IF mice.
855 n=4. *, $P<0.05$, All data represent the means ± SEM. Statistical significance was
856 determined by unpaired two-tailed Student's *t* test.

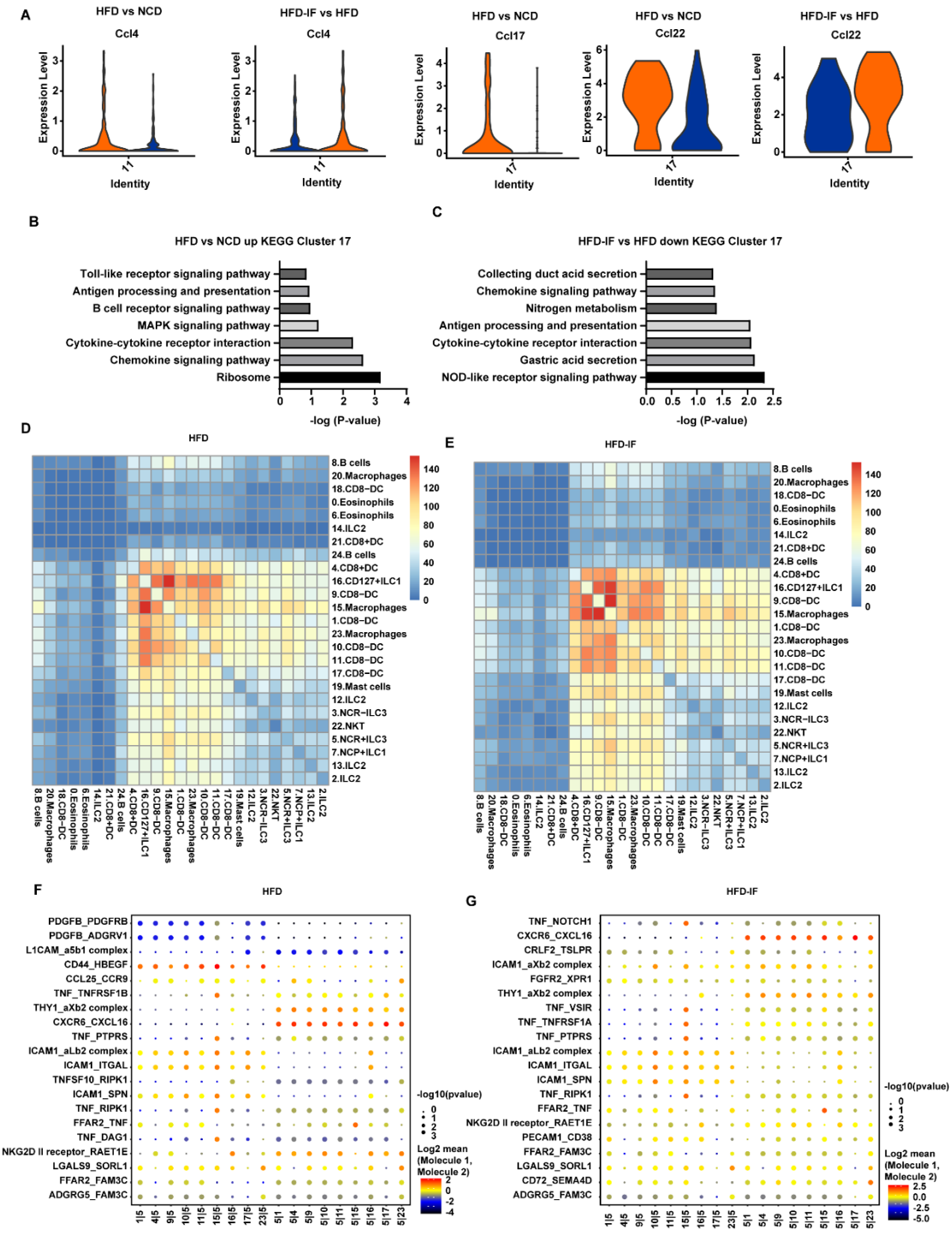

Fig. 7. Interaction between myeloid cells and ILC3s.

A. Violin plots showing the RNA expression of chemokines in CD8$^-$DCs (cluster 11 and cluster 17).

B. KEGG enrichment in upregulated genes of CD8$^-$DCs of HFD group compared with NCD group (cluster 17).

863 C. KEGG enrichment of downregulated genes of $CD8^-$DCs of HFD-IF group compared
864 with HFD group (cluster 17).
865 D. Heatmap showing the number of significant interactions identified between cell
866 types in sorted siLP immune cells of HFD mice as determined by Cellphone DB. The
867 color represents the number of interactions between cell types, a higher number of
868 interactions (red) and a lower number of interactions (blue).
869 E. Heatmap showing the number of significant interactions identified between cell
870 types in sorted siLP immune cells of HFD-IF mice as determined by Cellphone DB.
871 The color represents the number of interactions between cell types: a higher number of
872 interactions (red) and a lower number of interactions (blue).
873 F. Interaction pattern of the top 20 protein pairs and the top 20 cell types in sorted siLP
874 immune cells of HFD group mice. The x-axis is the cell type interaction, and the y-axis
875 is the protein interaction. The larger the point is, the smaller the p value. The color
876 represents the average expression, and red to black indicates the level from high to low.
877 G. Interaction pattern of the top 20 protein pairs and the top 20 cell types in sorted siLP
878 immune cells of HFD-IF mice. The x-axis is the cell type interaction, and the y-axis is
879 the protein interaction. The larger the point is, the smaller the p value. The color
880 represents the average expression, and red to black indicates the level from high to low.

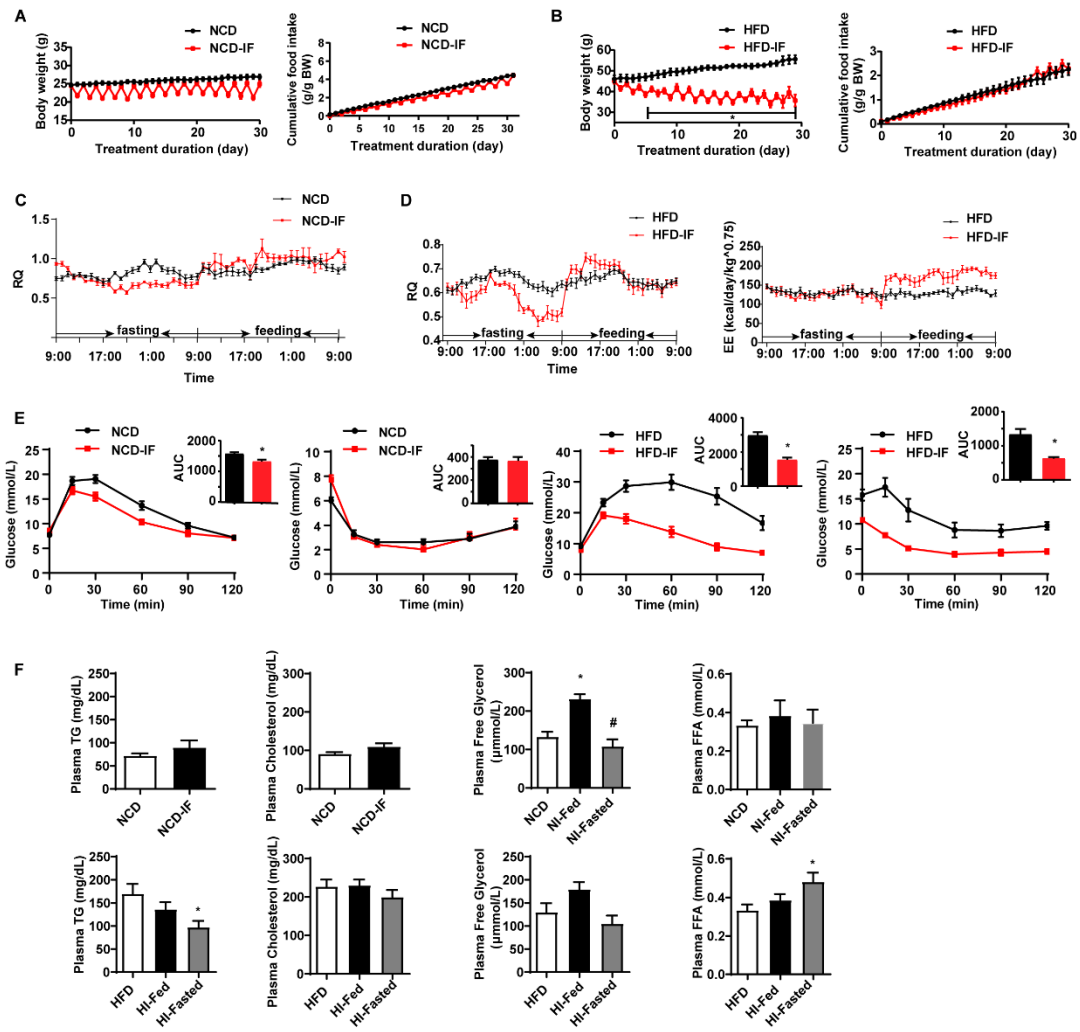

Supplementary Figure 1 Intermittent fasting improves glucose metabolism and lipid metabolism.

A. Body weight and cumulative food intake of mice fed NCD with or without intermittent fasting. n=9.

B. Body weight and cumulative food intake of mice fed HFD with or without intermittent fasting. n=9.

C. Respiratory quotient (RQ) of mice fed NCD with or without intermittent fasting. n=5.

D. Respiratory quotient (RQ), energy expenditure (EE) of mice fed HFD with or without intermittent fasting. n=5.

E. Oral glucose tolerance test (OGTT) and area under the curve (AUC). Insulin tolerance test (ITT) and area under the curve (AUC) of NCD, NCD-IF, HFD and HFD-IF mice. n=6 per group.

F. Levels of plasma triglycerides (TG), cholesterol, free glycerol and free fatty acids (FFA). n=6 mice/group.

All data represent the mean ± s.e.m. Statistical significance was determined by unpaired two-tailed Student's *t* test or one-way ANOVA with Bonferroni's multiple-comparisons test.

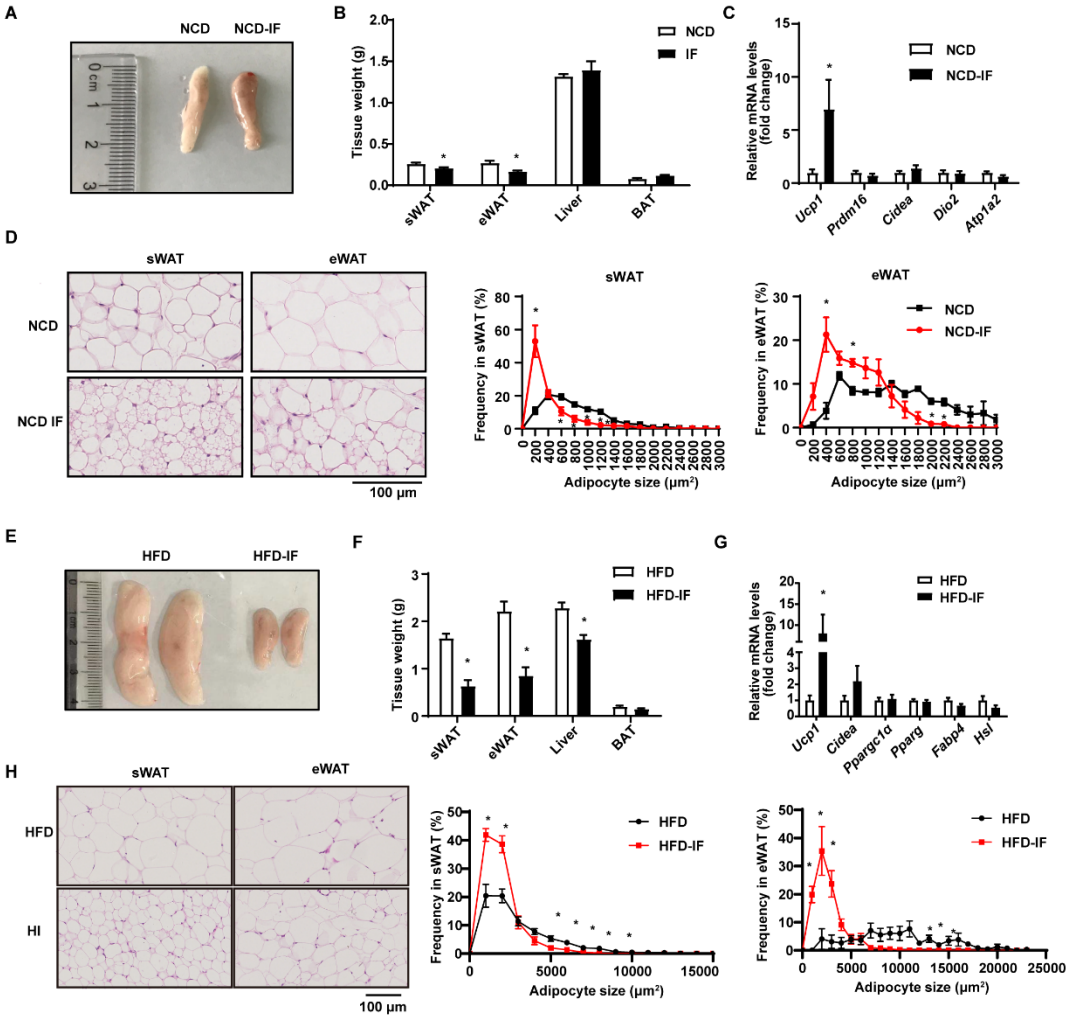

Supplementary Figure 2 Intermittent fasting promotes white adipose tissue

beigeing.

A. Representative image of sWAT from mice fed NCD with or without intermittent fasting.

B. Tissue weight of sWAT, eWAT, Liver, BAT,from NCD and NCD-IF mice. n=6.

C. qPCR analysis of thermogenic genes in sWAT from NCD and NCD-IF mice. n=6 mice/group.

D. H&E staining in sWAT and eWAT. Cell sizes were measured using ImageJ. n=5 per group. Scale bar: 100 μm.

E. Representative image for sWAT of HFD and HFD-IF mice. n=6.

F. Tissue weight of sWAT, BAT, Liver, eWAT from HFD and HFD-IF mice. n=6.

G. qPCR analysis of thermogenic genes in sWAT from HFD and HFD-IF mice. n=6 mice/group.

H. H&E staining in sWAT and eWAT from HFD and HFD-IF mice. Cell sizes were measured using ImageJ. n=5 per group. Scale bar: 100 μm.

All data represent the mean ± s.e.m. Statistical significance was determined by unpaired two-tailed Student's *t* test (A) or one-way ANOVA with Bonferroni's multiple-comparisons test (B).

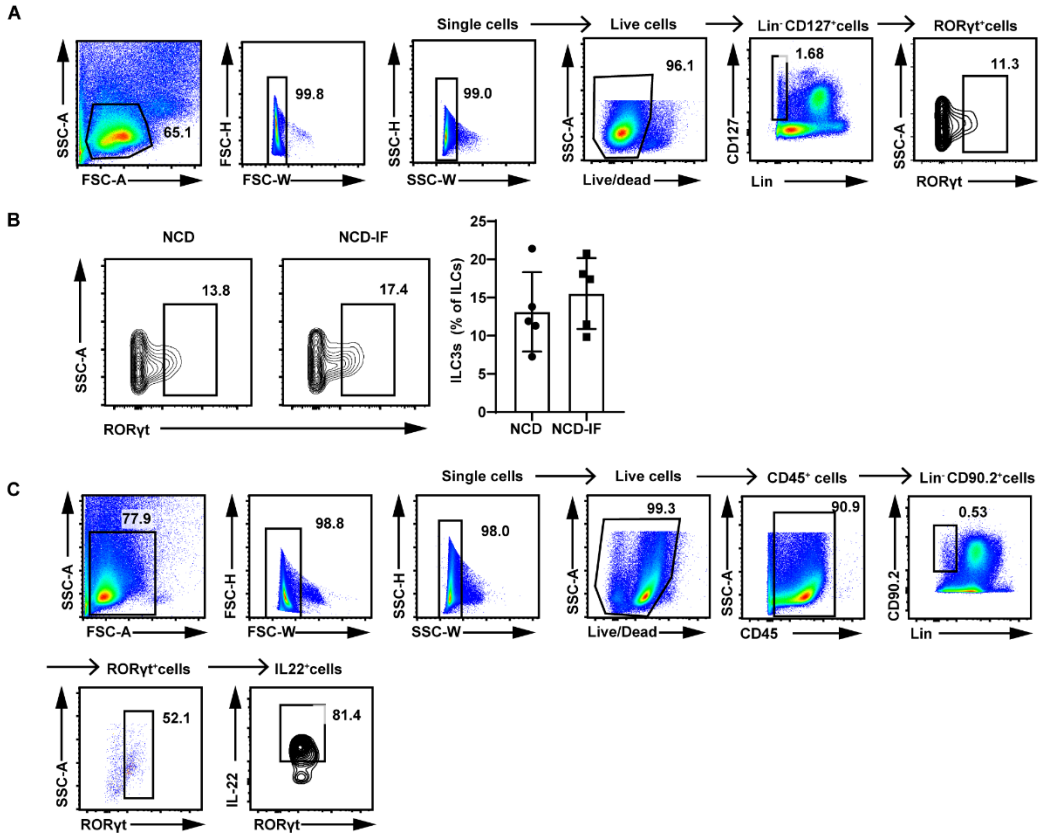

Supplementary Figure 3 Intermittent fasting demonstrates no effect on the number of ILC3s in sWAT.

A. Gating strategy for flow cytometry analysis of live lineage^{-}CD127^{+}RORγt^{+}ILC3s in the SVF of sWAT.

B. Flow cytometric analysis of RORγt+ ILC3s in live CD127^{+} lineage^{-} ILCs from the sWAT of NCD mice, NCD-IF mice. n=5.

C. Gating strategy for flow cytometry analysis of IL-22^{+} cells in live CD45^{+}lineage^{-}CD90.2^{+}RORγt^{+}ILC3s in the SVF of sWAT.

All data represent the mean ± s.e.m. Statistical significance was determined by unpaired two-tailed Student's *t* test.

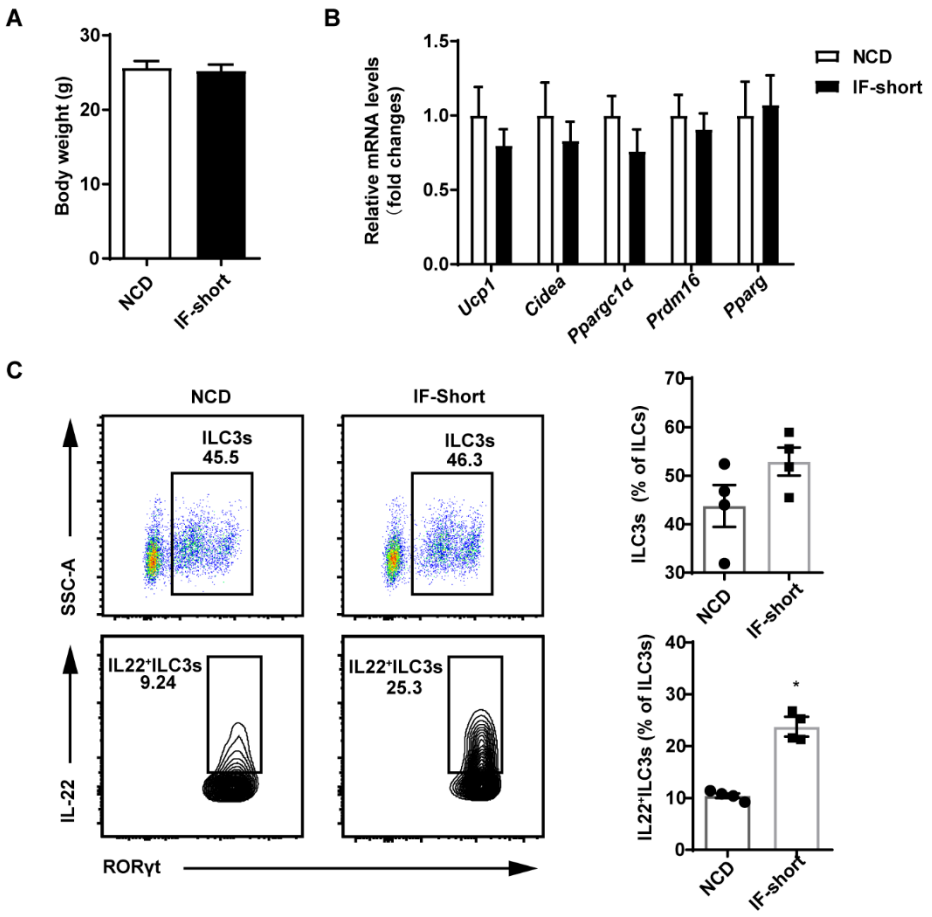

Supplementary Figure 4 Short-term intermittent fasting induces intestinal ILC3s to secrete IL-22.

Eight-week-old SPF mice were exposed to one cycle of intermittent fasting for 2 days (IF-short), while the control group (NCD) has free access to NCD. n=6.

A. Body weight of NCD and IF-short mice. n=6.

B. qPCR analysis of thermogenic genes in sWAT from NCD and IF-short mice. n=6 mice/group.

C. Flow cytometric analysis of RORγt^{+} ILC3s in live CD127^{+} lineage^{-} ILCs in the small intestine lamina propria of NCD or IF-short mice. Flow cytometric analysis of IL-22^{+} cells in live CD127^{+} lineage^{-} RORγt^{+} ILC3s from the small intestine lamina propria of

940 NCD or IF-short mice. Four independent experiments were performed with similar

941 results. n=4.

942 All data represent the mean ± s.e.m. Statistical significance was determined by unpaired

943 two-tailed Student's *t* test.

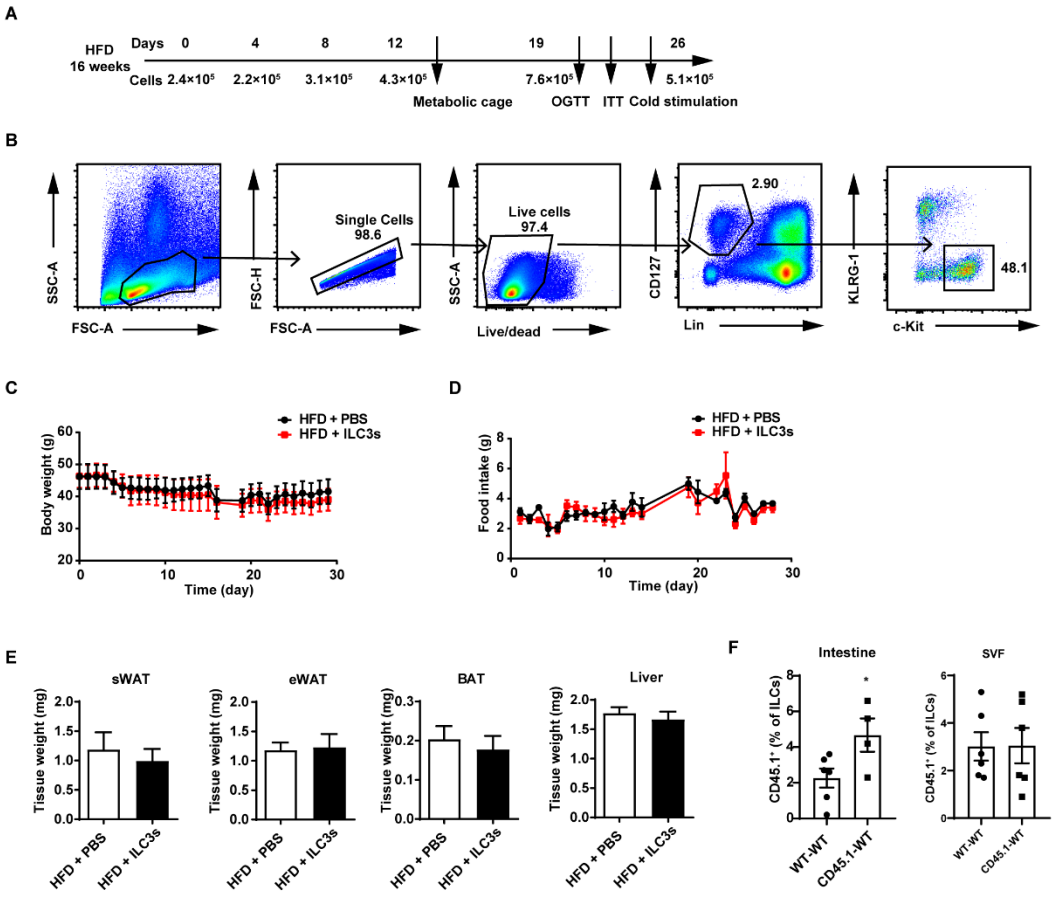

944

945 **Supplementary Figure 5 Adoptive transfer of ILC3s has no effect on the body**

946 **weight in mice fed HFD.**

947 A. Timeline for the recipient mice transferred with PBS or ILC3s. Mice were fed with

948 HFD for 16 weeks and then injected with ILC3s intravenously six times in a month.

949 B. Gating strategy for flow sorting of live CD127^{+} lineage^{-} c-kit^{+} KLRG1^{-}ILC3s in the

950 siLP.

C. Body weight of HFD mice transferred with ILC3s or control. n=6 per group.

D. Food intake of HFD mice transferred with ILC3s or control. n=6 per group.

E. Tissue weight of sWAT, eWAT, BAT, and liver from HFD mice transferred with ILC3s or control. n=6 per group.

F. Transfer of ILC3s from CD45.1 mice to WT mice. The percentage of CD45.1+ cells in ILCs in the small intestine and SVF. n=4-6.

All data represent the mean ± s.e.m. Statistical significance was determined by unpaired two-tailed Student's *t* test.

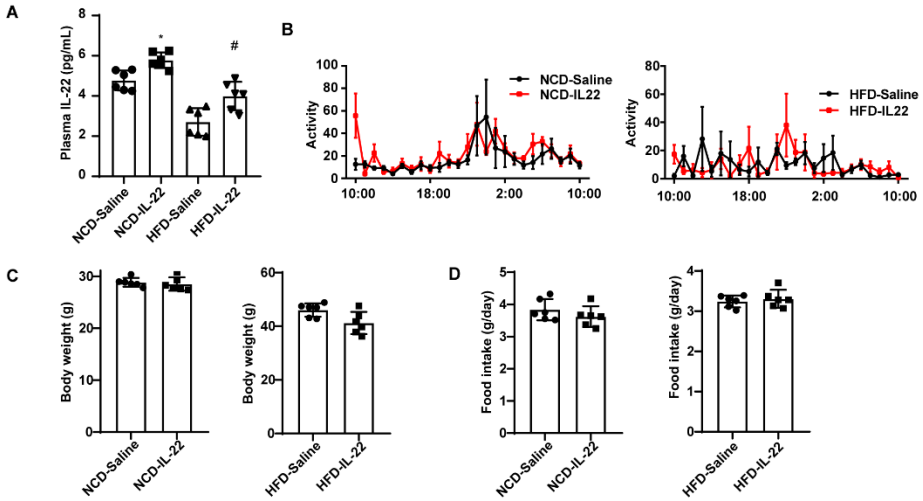

Supplementary Figure 6 Exogenous IL-22 has no effect on the body weight of mice.

A. Levels of IL-22 in plasma of NCD-Saline, NCD-IL-22, HFD-Saline, HFD-IL-22 mice. n=6 mice/group. # vs HFD-Saline.

B. Activity of mice fed NCD or HFD which were intraperitoneally injected with IL-22 or saline. n=5 for each group.

C. Body weight of NCD and HFD mice intraperitoneally injected with IL-22 or saline. n=6 for each group.

D. Daily food intake of NCD and HFD mice intraperitoneally injected with IL-22 or

968 saline. n=6 for each group.

969 F. Quantification of adipocyte size in sWAT and eWAT of mice with or without

970 intermittent fasting. Size of adipocytes were determined with ImageJ.

971 All data represent the mean ± s.e.m. Statistical significance was determined by one-

972 way ANOVA (A) with Bonferroni's multiple-comparisons test or unpaired two-tailed

973 Student's *t* test (B-D).

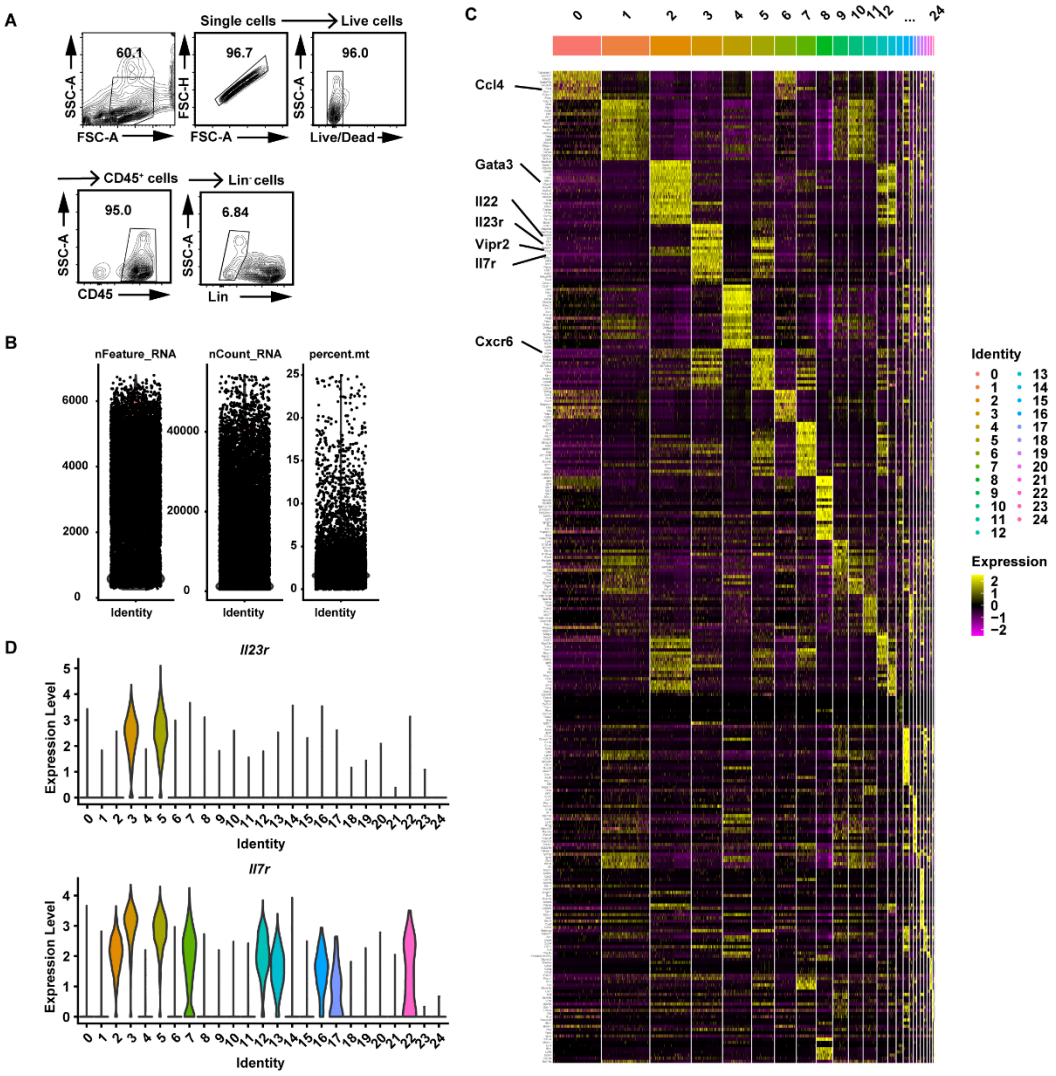

974

975 **Supplementary Figure 7 Profiling of intestinal immune cells from mice fed NCD,**

976 **HFD or HFD-IF**

977 A. Gating strategy for flow cytometry sorting of Live CD45^{+} Lineage^{-} immune cells in

978 the small intestine lamina propria.

979 B. scRNA-seq data quality control of sorted immune cells from mice fed NCD, HFD

980 or HFD-IF.

981 C. Unbiased heatmap of the gene levels of the top 20 unique cluster marker genes for

982 each cell cluster. Cluster identities are shown above the heatmap.

983 D. Violin plots showing RNA expression of cluster markers for the indicated cell

984 populations. UMAP feature plots are based on the UMAP shown in Figure 6A.

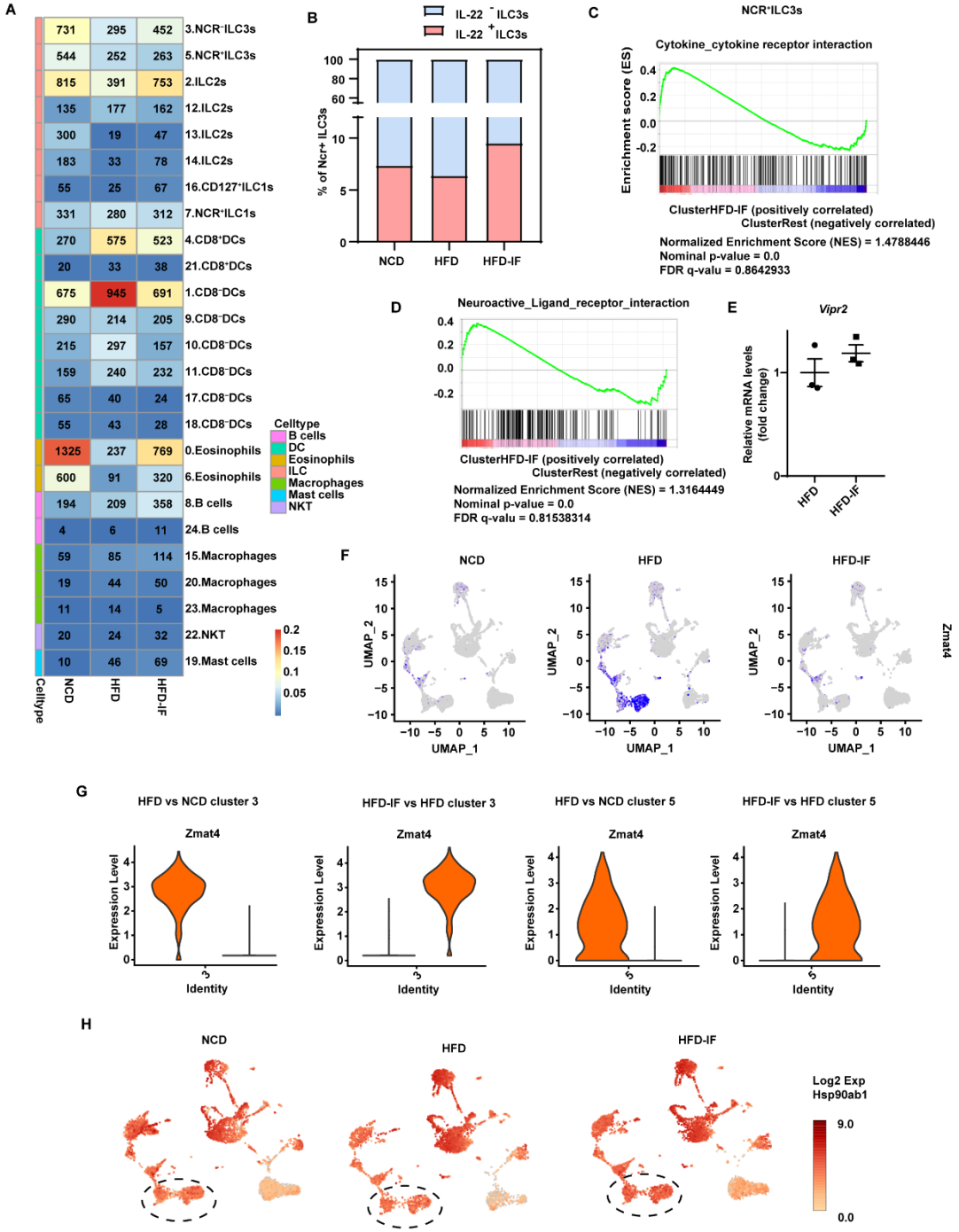

Supplementary Figure 8 Effects of Intermittent fasting on the gene expression of ILC3s.

A. Number and proportion of cells detected in each group in the study. Shown are Fraction (color bar, out of all cells from that group) and number of cells from each of the 25 cell clusters (rows) in each individual group (columns).

991 B. Percentage of IL-22^{+} cells defined by the mRNA levels using Loupe Browser 5.0 of
992 NCR^{+} ILC3s in NCD, HFD and HFD-IF mice.
993 C. GSEA demonstrating enrichment of cytokine-cytokine receptor interaction pathway
994 genes upregulated by intermittent fasting (HFD-IF mice) vs. control (HFD mice) in
995 NCR^{+} ILC3s.
996 D. GSEA demonstrating enrichment of neuroactive ligand-receptor interaction pathway
997 genes upregulated by intermittent fasting (HFD-IF mice) vs. control (HFD mice) in
998 NCR^{+} ILC3s.
999 E. qPCR analysis of *Vipr2* in ILC3s sorted from siLP of HFD or HFD-IF mice.
1000 F. UMAP feature plots showing RNA expression of Zmat4 based on the UMAP shown
1001 in Figure 6B.
1002 G. Violin plots showing RNA expression of Zmat4 in NCR^{-}ILC3s (cluster 3) and
1003 NCR^{+}ILC3s (cluster 5).
1004 H. UMAP feature plots showing RNA expression of Hsp90ab1 based on the UMAP
1005 shown in Figure 6B.

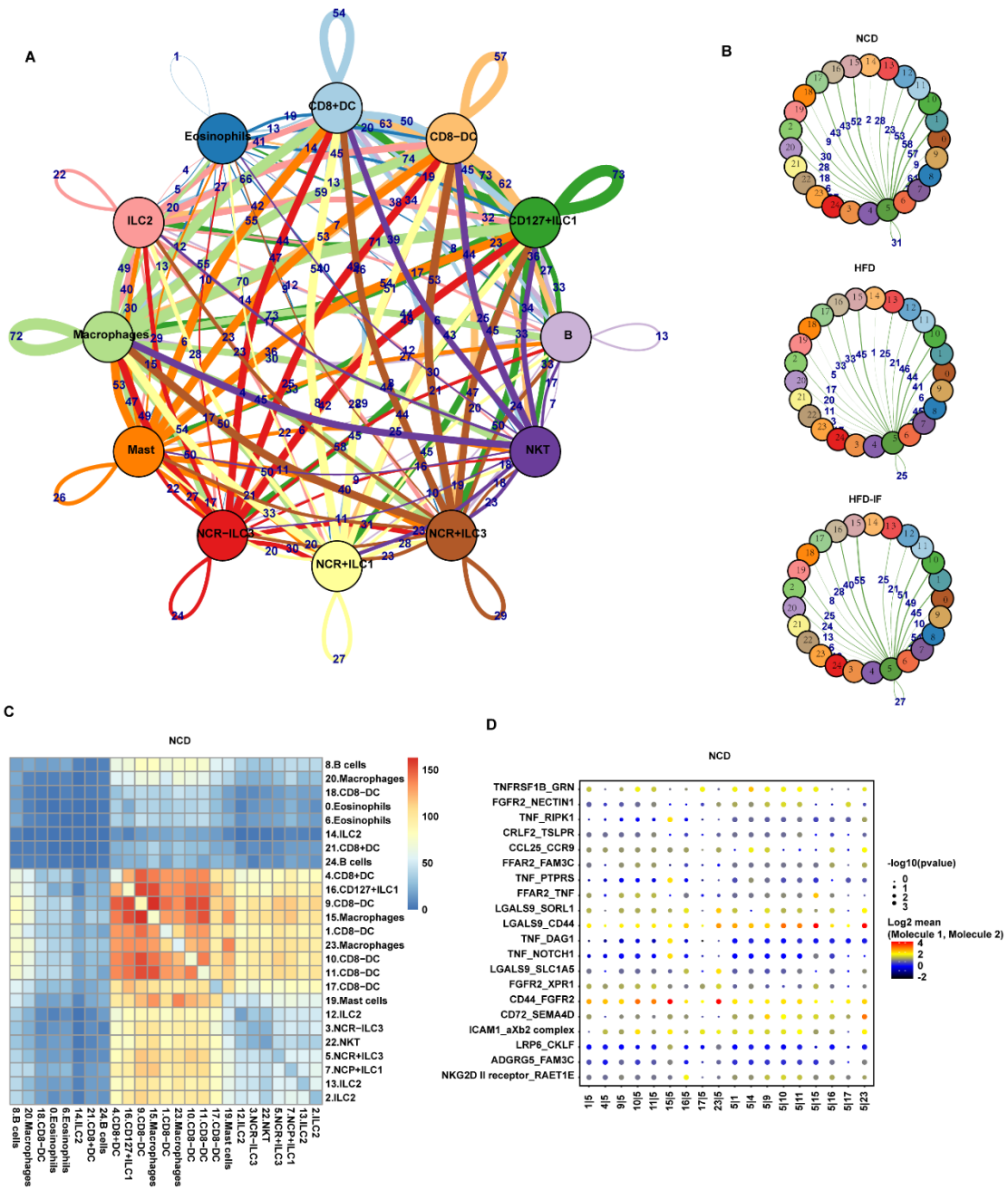

Supplementary Figure 9 Cell–cell interactions in the intestine.

A. Connectome web analysis of intestine immune cell interacting cell types based on the expression of the ligand in mice fed NCD. The vertex (colored cell node) represents the cell cluster. The thickness of the connecting lines is proportional to the number of interactions between the nodes.

B. Connectome web analysis of NCR^{+} ILC3s with the 25 cell clusters based on

expression of the ligand. The vertex (colored cell node) represents the cell cluster, while the thickness of the connecting lines is proportional to the number of interactions between two nodes.

C. Heatmap showing the number of significant interactions identified between cell types in sorted siLP immune cells of NCD mice as determined by CellphoneDB. The color represents the number of interactions between cell types: a higher number of interactions (red) and a lower number of interactions (blue).

D. Interaction pattern of the top 20 protein pairs and the top 20 cell types. The x-axis is the cell type interaction, and the y-axis is the protein interaction. The larger the point is, the smaller the p value. The color represents the average expression. Red to black indicates the level from high to low.

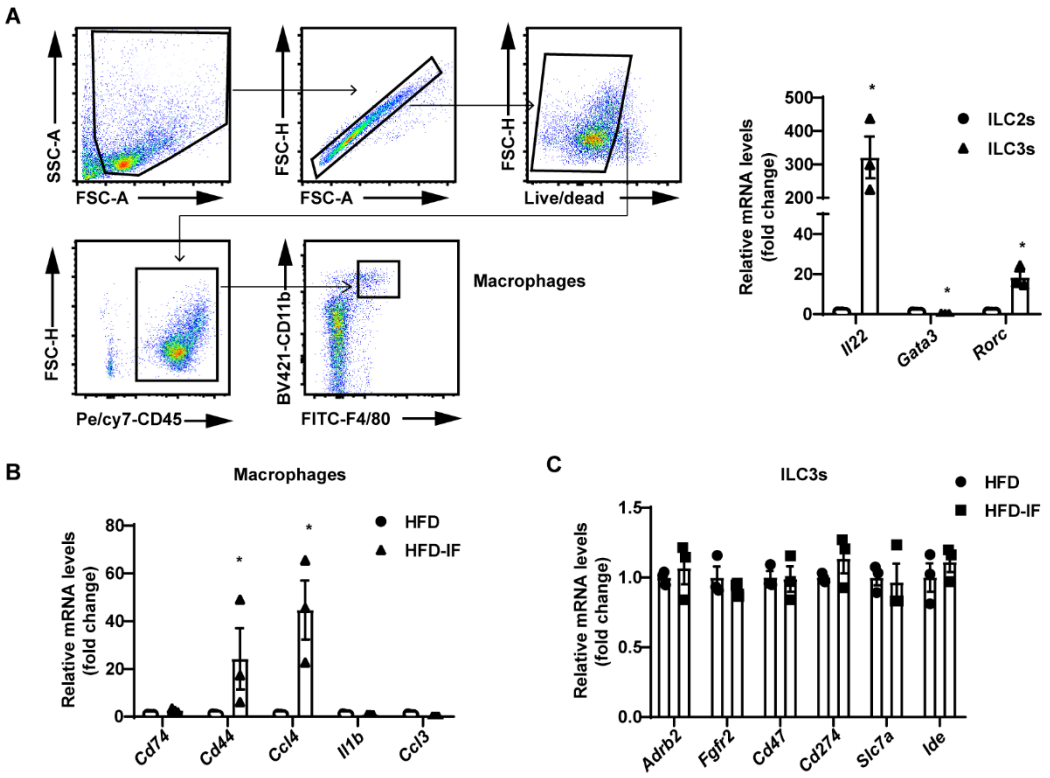

Supplementary Figure 10 Increased expression of CD44 and CCl4 in macrophages.

1026 Flow cytometry sorted macrophages and ILC3s from HFD and HFD-IF mice were used
1027 to detect the mRNA levels of proteins involved in the interaction of macrophages and
1028 ILC3s.
1029 A. Gating strategy for flow sorting of macrophages in the siLP. qPCR analysis of *Il22*,
1030 *Gata3*, and *Rorc* in ILC2s and ILC3s. n=3/group.
1031 B. mRNA levels of proteins involved in the interaction in macrophages. n=3/group.
1032 C. mRNA levels of proteins involved in the interaction in ILC3s. n=3/group.
1033 All data represent the mean ± s.e.m. Statistical significance was determined by unpaired
1034 two-tailed Student's *t* test.
1035
1036 **Table S1. Sequences of primers used in quantitative PCR.**

Gene	**Forward Primer**	**Reverse Primer**
Il22	ATGAGTTTTTCCCTTATGGGGAC	GCTGGAAGTTGGACACCTCAA
Il17	TCCCTCTGTGATCTGGGAA	CTCGACCCTGAAAGTGAAGG
Il1β	CCTTCCAGGATGAGGACATGA	TGAGTCACAGAGGATGG-GCTC
Il6	TAGTCCTTCCTACCCCAATTTCC	TTGGTCCTTAGCCACTCCTTC
Ifnγ	ATGAACGCTACACACTGCATC	CCATCCTTTTGCCAGTTCCTC
Tbp	ACCTTATGCTCAGGGCTTGG	GCCGTAAGGCATCATTGGAC
RpL32	GAGCAACAAGAAAACCAAGCA	TGCACACAAGCCATCTACTCA
Hprt2	TCAGTCAACGGGGGACATAAA	GGGGCTGTACTGCTTAACCAG
Hsl	CCAGCCTGAGGGCTTACTG	CTCCATTGACTGTGACATCTCG
Adrb3	GGCCCTCTCTAGTTCCCAG	TAGCCATCAAACCTGTTGAGC
Chrebpβ	AGATGGAGAACCGACGTATCA	ACTGAGCGTGCTGACAAGTC

Dio2	AATTATGCCTCGGAGAAGACCG	GGCAGTTGCCTAGTGAAAGGT
Atp1a2	CCACCACTGCGGAAAATGG	GCCCTTAGACAGATCCACTTGG
Atgl	AACACCAGCATCCAGTTCAA	GGTTCAGTAGGCCATTCCTC
Fabp4	ACACCGAGATTTCCTTCAAACTG	CCATCTAGGGTTATGATGCTCTTCA
Cidea	ATCACAACTGGCCTGGTTACG	TACTACCCGGTGTCCATTTCT
Ppargc1α	GATTGAAGTGGTGTAGCGAC	GTCGCTACACCACTTCAATC
Pparg	TCAGCTCTGTGGACCTCTCC	ACCCTTGCATCCTTCACAAG
Adrb3	GGCCCTCTCTAGTTCCCAG	TAGCCATCAAACCTGTTGAGC
Prdm16	CAGCACGGTGAAGCCATTC	GCGTGCATCCGCTTGTG
Il4	GGTCTCAACCCCCAGCTAGT	GCCGATGATCTCTCTCAAGTGAT
Ucp1	CACCTTCCCGCTGGACACT	CCCTAGGACACCTTTATACCTAATGG
Il23a	ATGCTGGATTGCAGAGCAGTA	ACGGGGCACATTATTTTTAGTCT
Tnf	CGTCGTAGCAAACCACCAAG	GAGATAGCAAATCGGCTGACG
Adrb2	GGGAACGACAGCGACTTCTT	GCCAGGACGATAACCGACAT
Fgfr2	CCTCGATGTCGTTGAACGGTC	CAGCATCCATCTCCGTCACA
Cd47	TGGTGGGAAACTACACTTGCG	CGTGCGGTTTTTCAGCTCTAT
Cd274	GCTCCAAAGGACTTGTACGTG	TGATCTGAAGGGCAGCATTTC
Slc7a1	CTGCCTCAACACCTATGACCT	GAGAGCAGCAATCAAGAAGGAG
Ide	AATCCGGCCATCCAGAGAATA	GGGTCTGACAGTGAACCTATGT
Cd74	AGTGCGACGAGAACGGTAAC	CGTTGGGGAACACACACCA
Cd44	TCGATTTGAATGTAACCTGCCG	CAGTCCGGGAGATACTGTAGC
Ccl4	TTCCTGCTGTTTCTCTTACACCT	CTGTCTGCCTCTTTTGGTCAG

Il1b	GCAACTGTTCCTGAACTCAACT	ATCTTTTGGGGTCCGTCAACT
Ccl3	TTCTCTGTACCATGACACTCTGC	CGTGGAATCTTCCGGCTGTAG
Gata3	CTCGGCCATTCGTACATGGAA	GGATACCTCTGCACCGTAGC
Rorγt	GACCCACACCTCACAAATTGA	GACCCACACCTCACAAATTGA

1037

1038 **Table S2. Key resources**

Antibody and clone	**Source**	**cat#**
Cell Staining Buffer	BioLegend	420201
eBioscience™ Fixation/Perm Diluent	Invitrogen	00-8333-56
eBioscience™ Fixable Viability Dye eFluor™ 606	Invitrogen	65-0866-14
PerCP/Cy5.5 anti-mouse CD45(30-F11)	BioLegend	103131
FITC anti-mouse CD3ε(RA3-6B2)	BioLegend	103205
FITC anti-mouse/human CD45R/B220(RA3-6B2)	BioLegend	103205
FITC anti-mouse Ly-6G/Ly-6C(Gr-1)(RB6-8C5)	BioLegend	108405
FITC anti-mouse CD19(6D5)	BioLegend	115506
FITC anti-mouse CD5(53-7.3)	BioLegend	100605
BV421 anti-mouse CD127(IL-7Rα) (A7R34)	BioLegend	135023
PE/Cyanine7 anti-mouse CD90.2(30-H12)	BioLegend	105325
PE/Cyanine7 anti-mouse CD45.1	BioLegend	110729
PE anti-mouse RORγt(Q31-378)	BD Pharmingen	562607
Alexa Fluor 647 anti-mouse IL-22(Poly5164)	BioLegend	516406
BV605 anti-mouse/human KLRG1(MAFA)(2F1/KLRG1)	BioLegend	138419
PE anti-mouse CD117(c-kit) (2B8)	BioLegend	105807
Rb pAb to UCP1	abcam	ab10983

1039